Influence of Spatial Rainfall Gradients on River Longitudinal Profiles and the Topographic Expression of Spatio-temporally Variable Climate in Mountain Landscapes

Joel S. Leonard[1] and Kelin X. Whipple[1]

[1]School of Earth and Space Exploration, Arizona State University, Tempe, Arizona, USA

Corresponding Author: Joel S. Leonard (joel.leonard@asu.edu)

Key Points

- Spatially variable rainfall complicates steady state relationships between mean rainfall and conventional topographic and erosion metrics.
- Transient responses to changes in rainfall pattern differ from uniform changes in rainfall, which affects how they may be detected.
- Rainfall gradients can obscure the sensitivity of fluvial erosion to rainfall variations and impede quantification of climate sensitivity.

Keywords: *River Profiles, Stream Power Model, Orographic Rainfall, Erosional Efficiency, Erosion Rates, Channel Steepness*

Abstract

Mountain landscapes have dynamic climates that, together with tectonic processes, importantly influence their topographic evolution. While spatio-temporal changes in rainfall are ubiquitous in these settings, their influence on river incision has been little studied. Here, we investigate how changes in rainfall pattern should affect both the steady state form and transient evolution of river profiles at the catchment scale using the stream power model. We find that non-uniform rainfall patterns complicate steady state relationships among conventional catchment-wide metrics like mean rainfall, channel steepness, and fluvial relief, which can influence the apparent sensitivity of landscapes and erosion rates to rainfall variations. We also find that transient responses to changes in rainfall pattern have an inherently multi-stage nature that importantly differs from expected responses to uniform changes in rainfall. This has several important implications, specifically for detecting transient responses to changes in rainfall pattern (and more broadly climate) in natural settings, and for interpretations of landscape morphometrics above

and below transient knickpoints. We find that disparate responses by rivers and river segments that experience different rainfall conditions, particularly trunk and tributary rivers, are an important factor in understanding catchment-wide responses, and accounting for such disparities may be important for detecting and quantifying landscape sensitivity to rainfall variations. Lastly, we show how explicitly accounting for rainfall patterns in channel steepness calculations, and thus variations in erosional efficiency, may be a necessary step toward overcoming challenges related to rainfall variations, and thus ultimately for advancing understanding of landscape sensitivity to climate in mountain settings.

Plain Language Summary

Mountain landscapes typically experience different amounts of rainfall with increasing elevation. It is widely thought that such differences should have a fundamental role in controlling the efficiency of erosional processes. This is particularly true for river erosion, which is the dominant erosional process shaping topography of most unglaciated mountain landscapes, because their erosive power is related to the amount and rate of discharge. However, much of our understanding about how rainfall influences the efficiency of river erosion, and how rivers adjust their form to accommodate changes in rainfall as climate changes with time, is based in a framework that compares the effects of different amounts rainfall. This framework typically assumes rainfall is uniformly distributed in the river basin, and therefore neglects the influence of spatially variable rainfall that mountain rivers typically experience. We find that even modest along-stream variations in rainfall can complicate common expectations about how topography should reflect differences in rainfall. Expectations about how rivers adjust to changes in rainfall pattern, and more broadly to changes in climate, are similarly affected. These findings have important implications for recognizing both the influence of modern spatial variations in climate on active landscape processes and ongoing adjustments to past climate changes.

1. Introduction

1.1 Motivation

Advances in tectonic geomorphology require quantitative understanding about relationships among climate, tectonics, and erosion. In temperate mountain landscapes, studies of bedrock rivers provide important insights into interactions between these processes (e.g., D'Arcy & Whittaker, 2014; Harel et al., 2016; Kirby & Whipple, 2012; Lague, 2014; Olen et al., 2016; Scherler et al., 2017; Kelin X Whipple & Tucker, 1999; Whittaker, 2012). However, despite longstanding theoretical support for the notion that climate, like tectonics, has a fundamental role influencing erosion (e.g., Bonnet & Crave, 2003; Howard & Kerby, 1983; Lague, 2014; Molnar, 2001; Perron, 2017; Rinaldo et al., 1995; Tucker & Slingerland,

1997), a direct, general relationship between climate and erosion has proven elusive (Perron, 2017; Whittaker, 2012). In this paper, we explore the extent to which this conundrum may reflect limitations in the current framework describing how climate-related signals should be expressed in landscapes that, in turn, may impede recognition of diagnostic characteristics of landscape response to climate change.

Orographic precipitation patterns are ubiquitous in mountain landscapes. In general, they develop from the interaction of humid air masses with topographic relief (see Roe, 2005 for an overview), and can create dramatic spatial and elevation dependent gradients in precipitation. While numerous factors affect orographic precipitation patterns in detail, broadly speaking, atmospheric moisture content and topographic characteristics (e.g., relief) are primary physical controls on their development (e.g., Held & Soden, 2006; Roe, 2005; Roe et al., 2008; Trenberth et al., 2003). Because atmospheric moisture content depends strongly on temperature (i.e., Clausius-Clapeyron relationship; Held & Soden, 2006; Roe, 2005; Trenberth et al., 2003), shifts in temperature that accompany changes in climate must influence these precipitation patterns. Therefore, if erosional processes in these landscapes are generally sensitive to variations in precipitation, then changing characteristics of orographic precipitation patterns (e.g., strength of rainfall gradients) with changes in climate should importantly influence mountain landscape evolution.

In mountainous settings, transverse rivers tend to cross orographic precipitation gradients, which are generally oriented orthogonally to the topographic trend of the range. Their tributaries, on the other hand, typically experience a relatively muted range in precipitation due to their orientation and/or smaller areal extent. Consequently, rivers of different size, orientation, and position often experience dramatically different precipitation conditions. Within large river basins, these differences may be substantial. Exposure to orographic precipitation patterns is expected to systematically affect river profile concavity; increases in precipitation with distance upstream lowers profile concavity, while the opposite trend increases profile concavity (Han et al., 2014, 2015; Roe et al., 2002, 2003; Ward & Galewsky, 2014). Importantly, this implies that adjustment to a change in orographic precipitation pattern should involve longitudinally variable amounts of incision (i.e., transient changes in concavity). Furthermore, because transverse rivers set erosional base level for their tributaries, any along-stream variation in incision exhibited by transverse rivers as they adjust will necessarily drive spatially and temporally variable base level histories for tributaries. Developing a framework that accommodates such variability and its influence on river profile evolution is a fundamental need.

1.2 Approach and Scope

In this paper, we investigate how spatio-temporal changes in precipitation may influence erosion and

topography of mountain landscapes using the stream power model (SPM). First, we show how simple spatial gradients in rainfall, resembling typical orographic rainfall gradients (i.e., increasing or decreasing downstream; herein referred to as bottom-heavy, and top-heavy, respectively), influence river profile form at steady state in one dimension. Then, we present a sensitivity analysis that characterizes how changes in rainfall pattern should affect the steady-state form of a given river profile. Following this, we use a quasi-two-dimensional numerical model to simulate the response of a transverse, trellised river network to a change in rainfall pattern, which we compare to better-understood spatially uniform changes in rainfall. Finally, we discuss some implications of these results for studies set in mountain landscapes. A comprehensive analysis of the co-evolution of orographic rainfall patterns and topography is beyond the scope of this paper. Instead, we focus on characterizing the controls on landscape response to imposed changes in rainfall patterns, highlighting where expectations differ from uniform changes in rainfall, and implications of those differences.

2. Methods

2.1 Model Description

Following Riihimaki et al., (2007), we use a quasi-two-dimensional finite difference model of bedrock channels to represent an idealized river basin. We abstract river basin topology to comprise a single one-dimensional trunk profile and 51 regularly spaced (1 km) one-dimensional tributary profiles. We model erosion as detachment-limited (Howard, 1994; Whipple & Tucker, 1999) following a general form of the SPM:

$$E = KA^m S^n, \tag{1a}$$

$$K = K_p \bar{P}^m, \tag{1b}$$

$$E = K_p Q^m S^n, \tag{1c}$$

where E is the erosion rate, K and K_p are erosional efficiency constants, A is upstream drainage area, S is the channel slope, $\overline{P}$ is the upstream average rainfall rate, Q is water discharge equal to $\overline{P}A$, and m and n are positive constant exponents (Table 1). We use $n = 2$ and $m = 1$ for all model runs as values of $n > 1$ appear more appropriate in many settings (e.g., Adams et al., 2020; Harel et al., 2016; Lague, 2014). First-order results do not rely on choices of m or n providing the ratio between the two is maintained, but the nonlinear dependence of erosion rate on slope (i.e., $n = 2$) affects details of the transient behavior, and because $m = 1$, note that K is directly proportional to both $\overline{P}$ and Q. We explicitly treat the influence of climate on erosional efficiency (e.g., Adams et al., 2020; Roe et al., 2003) such that K_p is independent of

rainfall, but still encapsulates a number of factors including rock properties and details of erosional processes (Royden & Perron, 2013; Whipple & Tucker, 1999). Rock uplift rate (U) and K_p are spatially and temporally uniform for the duration each model run, and invariant across model runs. We define drainage area (A) for both the trunk and tributary profiles following Hack, (1957):

$$A = k_a x^h + A_c, \quad (2)$$

where x is distance along the channel downstream from the channel head, k_a and h are constants, and A_c is the upstream drainage area at the channel head – equal to 1 km^2. Channel length (L) and drainage area are fixed for each profile, and do not evolve over the course of a model run (Table 1). Discharge (Q) is calculated at each profile node from equation (2) as:

$$Q = \overline{P}A. \quad (3)$$

This definition assumes the simplest hydrological condition where all rainfall is converted directly to runoff. Discharge does not pass from tributaries to the trunk river as drainage area along the trunk is set by equation (2) independently. This approach allows closely spaced tributaries with uniform characteristics to better describe erosional response while maintaining empirically supported scaling between channel length and drainage area throughout the modelled river basin. Tributary outlets are fixed to the elevation of the trunk profile at their confluence. Importantly, this means that while there is not two-dimensional hydrological coupling through discharge, transient signals are communicated from the trunk to tributaries through variations in base level.

The initial condition for all models is steady state with spatially uniform rainfall. For simplicity, we model orographic precipitation exclusively as constant gradients in rainfall (i.e., linear changes with distance) that span the length of the trunk river (and orthogonal to tributaries). Imposed changes in rainfall evolve linearly over the first 10 kyr of model time. Tributary profiles are modeled with spatially uniform rainfall set by their position along the trunk profile; thus, individual tributaries experience spatially uniform changes in rainfall as orographic gradients evolve. This simplification is consistent with the notion that, due to their smaller areal extent and orientation, tributaries set within mountain-belt scale orographic gradients experience relatively uniform rainfall.

2.2 Analysis of River Profiles and Erosion Rates

We quantify river profile form and responses to changes in rainfall patterns using channel steepness

metrics and erosion rates. These metrics are commonly used, and often in tandem, to study influences of climate and/or tectonics in mountain settings (Adams et al., 2020; Bookhagen & Strecker, 2012; Cyr et al., 2014; DiBiase et al., 2010; Duvall, 2004; Godard et al., 2014; Insel et al., 2010; Kober et al., 2015; Morell et al., 2015; Olen et al., 2016; Ouimet et al., 2009; Portenga et al., 2015; Safran et al., 2005; Scherler et al., 2014; Vanacker et al., 2015; Willenbring et al., 2013).

Within the SPM framework, river slope is directly related to its erosional capacity (Equations 1a, 1c). A frequently applied metric in mountain landscapes that accounts for the general covariation between slope and drainage area is a normalized channel steepness index, k_{sn}:

$$k_{sn} = SA^{\theta_{ref}}, \tag{4}$$

where θ_{ref} is the reference concavity index (Wobus et al., 2006). We use a value of θ_{ref} = 0.5, which is consistent with common usage in natural landscapes and with SPM predictions that $\theta_{ref} = m/n \approx 0.5$ where rock uplift rate (U) and erosional efficiency (K) are uniform (Tucker & Whipple, 2002). As previously noted, the SPM predicts that orographic rainfall gradients should produce longitudinal variations K (Equation 1b) that, in turn, affect the concavity index, θ (Han et al., 2014, 2015; Roe et al., 2002, 2003). Any such variations are systematically reflected in the spatial pattern of k_{sn} and $\theta \neq \theta_{ref}$ is expected. Importantly, however, many studies relate upstream-average values of k_{sn} to measured spatially-averaged erosion rates, which relies on quasi-uniform (or linear) upstream k_{sn} to be valid (Wobus et al., 2006). Therefore, in cases where systematic longitudinal variations in K affect the downstream pattern of k_{sn} (i.e., upstream k_{sn} varies non-linearly), the meaning of such an average is not obvious.

To address complications introduced by rainfall gradients, we use discharge rather than drainage area to calculate channel steepness to arrive at $k_{sn\text{-}q}$ (Adams et al., 2020):

$$k_{sn-q} = SQ^{\theta_{ref}}. \tag{5}$$

We note, $k_{sn\text{-}q}$, like k_{sn}, is an empirically supported metric independent from the SPM. In principle, however, $k_{sn\text{-}q}$ is analogous to Erosion Index (EI) used by Finlayson et al., (2002) provided that $m/n \approx \theta_{ref}$, such that EI = $(k_{sn\text{-}q})^n$. Importantly, to the extent that the SPM captures the influence of discharge on erosional efficiency, it predicts that along-stream variations in $k_{sn\text{-}q}$ should scale with local erosion rate, much like it does for k_{sn} where K is spatially uniform. Hereafter, we use k_{sn} and $k_{sn\text{-}q}$ to refer to upstream averaged values, consistent with their common usage in analyses of catchment-mean erosion rates, unless we specifically state that they represent local values.

Millennial-scale catchment-averaged erosion rates measured, for example, using cosmogenically-derived ^{10}Be found in quartz in alluvial sediment (e.g. Bierman & Steig, 1996; Brown et al., 1995; Granger et al., 1996), seek to quantify erosion rates at the river basin scale. At steady state, spatially-averaged erosion rate, local incision rate, and rock uplift rate are equivalent; however, during periods of transient adjustment these values differ, complicating interpretations (Willenbring et al., 2013; Wobus et al., 2006). To make our results more portable to studies of natural landscapes, we calculate the spatially averaged erosion rate (E_{avg}) in addition to the instantaneous vertical incision rate (E):

$$E_{avg}{}_j = \left(\sum_{x_h}^{j}\left[E_j \cdot \left(A_j - A_{j-1}\right)\right]\right)/A_j, \quad (6)$$

where j corresponds to a downstream node of the profile, and x_h is the channel head.

3. 1-Dimensional Profiles

3.1 Influence of Longitudinal Rainfall Gradients on River Profiles at Steady State

Where rainfall is spatially uniform, topographic metrics (e.g., fluvial relief, channel steepness) are expected to vary inversely and monotonically with mean rainfall at steady state, but non-uniform rainfall patterns complicate these expectations. Steady state river profiles subjected to varying amounts of spatially uniform rainfall are shown in Figure 1a alongside discharge (Q) as a function of distance downstream for each profile, and corresponding relationships between mean rainfall ($\overline{P}$) and fluvial relief (R), k_{sn}, and $k_{sn\text{-}q}$. In comparison, Figure 1b shows a comparable suite of model steady state profiles subject to uniform, decreasing upstream, and increasing upstream rainfall patterns, that constitute an example where fluvial relief and k_{sn} actually increase with mean rainfall. This reversal reflects limitations of metrics like mean rainfall and k_{sn} where climate is spatially variable.

Systematic longitudinal variations in rainfall require that the mean (upstream average) rainfall values change systematically downstream, which in turn influences erosional efficiency (K) in a similarly systematic manner (Equation 1b), and thus equilibrium channel slope. Where such spatial variations exist, mean values of rainfall and k_{sn} therefore depend on where they are measured, which makes the meaning of a given value difficult to interpret. In contrast, to the extent that the SPM captures the influence of discharge on erosional efficiency, $k_{sn\text{-}q}$ is independent of changes in mean rainfall, as is shown in Figure 1. Comparison of SPM equations for k_{sn} and $k_{sn\text{-}q}$ at steady state ($E = U$) clearly shows this difference:

$$k_{sn} = \left(\frac{U}{K_p \bar{P}^m}\right)^{1/n}, \quad (7a)$$

$$k_{sn-q} = \left(\frac{U}{K_p}\right)^{1/n}. \quad (7b)$$

For spatially uniform rock uplift rate (U) and K_p, steady state fluvial relief (R) is proportional to the upstream integrated discharge (Han et al., 2015; Roe et al., 2003; Royden & Perron, 2013). Integrating equation (1c) from base level (x_b) upstream to the channel head (x_h), it can be shown that:

$$R = \left(\frac{U}{K_p}\right)^{1/n} \int_{x_b}^{x_h} Q^{-m/n}\, dx. \quad (8)$$

We point out that because fluvial relief depends on the cumulative effect of discharge (Q) it does not necessarily scale monotonically with discharge or rainfall measured at any single position, or averaged along any segment of a profile, except under the special condition where rainfall is spatially uniform (Gasparini & Whipple, 2014; Han et al., 2015). This alone suggests that quantifying the magnitude of temporal changes in mean rainfall (e.g., degree to which mean rainfall increases or decreases) is inadequate, at least under some conditions, to predict morphological responses of mountain landscapes to changing climate, or how a transient response may be expressed. Instead, how rainfall patterns have changed, and specifically, *where* rainfall has changed within a given catchment must be considered.

3.2 Transient River Profile Response to Spatio-temporal Changes in Rainfall Patterns

According to the SPM, transient responses to climate change are primarily driven by changes in discharge that, in turn, affect erosional efficiency. As orographic precipitation patterns change with changes in climate, different positions within a river basin may experience an increase or a decrease in rainfall. This spatial rainfall variability fundamentally affects how discharge accumulates, and ultimately how river profiles respond during transient adjustment.

Whether discharge locally increases or decreases following a change in rainfall pattern depends on how the rainfall pattern has changed upstream from a given position. (Hereafter we use subscripts *i* and *f*, respectively, to denote initial and final steady states, before and after a change in rainfall pattern.) As with spatially uniform changes in rainfall, local equilibrium channel slope varies inversely with discharge. While discharge is somewhat buffered from localized variations in rainfall by integrating upstream conditions, because discharge accumulates non-linearly downstream relatively modest rainfall gradients can have a strong influence on the downstream pattern. Notably, we find that a wide range of changes in rainfall patterns cause inversions in relative changes in discharge along a river. That is, while discharge may increase in upstream locations ($Q_f > Q_i$) for a given change in rainfall pattern, it may also decrease in

downstream locations ($Q_f < Q_i$), or vice versa.

Along-stream reversals in the relative change in discharge imply a position where discharge, and therefore also equilibrium slope, are unchanged ($Q_f = Q_i$ and $S_f = S_i$). We refer to this position as x_{sc}, and as we will show, changes in rainfall pattern that cause such reversals drive unique transient adjustments. For now, we note that upstream of x_{sc} initial and final steady state profiles begin to converge (see Figure 2). Thus, x_{sc} marks a local maximum difference between initial and final steady state profiles. This convergent behavior contrasts with expectations for spatially uniform changes in rainfall where the difference in channel bed elevation increases monotonically upstream from the outlet (Figure 1a).

Assuming spatially uniform rock uplift rate (U) and K_p, the magnitude of this difference along the profile between initial and final states, Δz_{Sc}, can be expressed:

$$\Delta z_{Sc} = \left(\frac{U}{K_p}\right)^{1/n} \int_{x_b}^{x_{sc}} \left(Q_f - Q_i\right)^{-m/n} dx. \quad (9)$$

In some circumstances, initial and final steady state profiles can intersect. The condition that determines whether this occurs can be similarly expressed:

$$0 = \left(\frac{U}{K_p}\right)^{1/n} \int_{x_b}^{x_{zc}} \left(Q_f - Q_i\right)^{-m/n} dx, \quad (10)$$

where x_{zc} is the position of intersection (Figure 2). Interestingly, x_{zc} marks a change in the net adjustment required to reach steady state (i.e., enhanced incision vs. surface uplift). Also, rainfall patterns that satisfy this condition are those that lead to positive relationships between mean rainfall and fluvial relief (Figure 1b). That is, these are changes in rainfall pattern where the SPM predicts an increase in mean rainfall would actually support growth of catchment topographic relief rather than a reduction, and vice versa.

3.3 Sensitivity Analysis of 1-D River Profiles to Spatio-temporal Changes in Rainfall Patterns

In this section, we present a sensitivity analysis to evaluate the influence of changes in rainfall pattern on discharge and fluvial relief compared to uniform changes in rainfall by exploring how different rainfall gradients should affect a given steady state river profile (Figure 3).

We define different fields bounding rainfall gradients that result in different classes of behavior (Figure

3a). Boundaries demarcating these fields are independent of U, K_p, m, and n provided m/n is unchanged. Channel length has a negligible influence for channels longer than a few kilometers where $A >> A_c$. The h exponent in Hack's relationship (Equation 2) can influence field boundaries, as indicated in Figure 3a; however, the effect is minor for the range of h values typically observed in nature (e.g., Rigon et al., 1996). Contours of Q_f/Q_i illustrate the extent to which a given rainfall gradient represents a net wetter ($Q_f/Q_i > 1$) or drier ($Q_f/Q_i < 1$) condition (Figure 3b). Contours of R_f/R_i describe the extent to which fluvial relief increases ($R_f/R_i > 1$) or decreases ($R_f/R_i < 1$). These contours show that steady state fluvial relief (R_f/R_i) is sensibly correlated with mean rainfall (Q_f/Q_i), but the relationship is complex when rainfall is not spatially uniform.

White fields (Figure 3, both panels) encompass rainfall gradients – and uniform changes in rainfall – where the entire profile would experience wetter or drier conditions. Transient adjustments to such gradients generally mimic adjustments to spatially uniform increases or decreases in rainfall, although non-uniform changes are expected to affect adjustments differently than uniform changes in detail.

Light grey fields (Figure 3a) encompass rainfall gradients that would produce x_{sc}, but not x_{zc}; thus, relative changes in discharge and equilibrium slope would invert along the profile, but initial and final steady state profiles would not intersect. During transient adjustment, the mode of transient adjustment is variable in space and time upstream of x_{sc} (variably $E > U$ or $E < U$; Figure 2). Despite this, the net change in fluvial relief caused by these changes is inversely related to the change in mean rainfall at steady state, consistent with expectations for spatially uniform changes in rainfall. Lastly, x_{sc} marks the position of the absolute maximum difference between initial and final steady states in these cases, not the channel head. Therefore, while the entire profile experiences net incision or surface uplift to reach steady state, the largest changes are along the central part of the profile.

Dark grey fields (Figure 3a) encompass rainfall gradients that produce both x_{sc} and x_{zc} and are characterized by the most complex transient responses. Implied relative differences in discharge and slope follow as for light grey fields, and modes of transient adjustment are similarly spatio-temporally variable upstream from x_{sc} (Figure 2). The distinguishing feature of these gradients is that the resulting steady state fluvial relief is positively related to the change in mean rainfall (e.g., Figures 1b, 2). The absolute maximum difference between initial and final steady states may either be at x_{sc} or at the channel head in these cases depending on specific characteristics of the change in rainfall gradient.

This analysis reveals several interesting ways that changes in rainfall pattern influence river profiles differently than expected for uniform changes. First, changes in longitudinal rainfall gradients that result

in complex transient responses (grey fields in Figure 3a) appear relatively common and do not require extreme changes in rainfall patterns. Note, we define our usage of 'complex transient responses' hereafter to include all responses that result in x_{sc} (i.e., both grey fields in Figure 3a), unless we specify otherwise. That these complex responses arise readily from a range of changes in rainfall patterns suggests that these types of responses may be a typical aspect of landscape evolution in mountain settings.

Our analysis also shows that among changes in rainfall pattern where a positive relationship between the change in mean rainfall and fluvial relief is expected (dark grey fields in Figure 3a), changes to top-heavy and bottom-heavy conditions have an asymmetric influence on fluvial relief. While top-heavy gradients in this category always inhibit growth of fluvial relief (R_f /R_i always < 1) and bottom-heavy gradients promote topographic growth, contour spacing of changes in fluvial relief show that incremental changes in bottom-heavy gradients have a stronger influence (Figure 3). This asymmetry follows directly from equation 8, and arises because higher rainfall in the headwaters of a catchment (top-heavy) influences equilibrium channel slope everywhere downstream, but higher rainfall near base level (bottom-heavy) does not influence channel slope upstream.

Testing a broad range of parameters that may be applicable to major mountain ranges (e.g., K_p, U, h, L), we find that changes in rainfall gradients alone may support increases or decreases in steady state fluvial relief by as much as 10^2–10^3 m in the opposite direction expected based on the change in mean rainfall assuming a uniform change (e.g., an increase in relief associated with an increase in mean rainfall). Simultaneously, the same change may drive as much as 10^1–10^2 m of enhanced incision or surface uplift along downstream and central portions of catchments consistent with conventional expectations for the change in mean rainfall. This spatially segregated behavior may be particularly important for understanding sediment transport out of mountain catchments and signals related to development of landforms like fluvial terraces, for example, which we do not treat in this paper but nevertheless warrants further research.

Lastly, we emphasize that the response to a change in rainfall pattern strongly depends on the initial conditions – we revisit this point in section 5.1. Together this analysis supports the notion that non-uniform changes in rainfall pattern can readily and importantly influence landscape form and processes in ways that fundamentally differ from expectations for spatially uniform changes in rainfall.

4. Transient Evolution of River Basins Responding to Changes in Rainfall Patterns

The transient response of a river basin to a change in rainfall pattern is highly dynamic. Fortunately, many

of the ideas laid out above for 1-dimensional profiles intuitively transfer to understanding how signals propagate through a simple trellis drainage network, albeit with some additional considerations. It is important to remember that trunk (transverse) rivers control base level for tributaries. Complex responses to changing rainfall patterns, like those described above where both the magnitude and mode of transient adjustment vary along the trunk profile in space and time, necessarily result in varying boundary conditions for tributaries. In addition, tributary responses to these variable base level signals are modulated by the rainfall history experienced by a given tributary, which is always different from the trunk. Finally, adjustments migrate upstream at a finite rate, so there is a time lag between a change in rainfall pattern and arrival of the associated base level signals from the trunk adjustment to a given tributary. The duration of this lag, as well as local rainfall conditions within a tributary catchment, are a function of its position along the trunk profile.

In the following, we explore the transient response of modelled trellis river basins to four representative climate change scenarios: (1) a spatially uniform decrease in rainfall, (2) a spatially uniform increase in rainfall, (3) a shift from spatially uniform rainfall to a bottom-heavy rainfall gradient, and (4) a shift from spatially uniform rainfall to a top-heavy rainfall gradient.

4.1 Case 1: Spatially Uniform Decrease in Rainfall

The modelled catchment response to a spatially uniform decrease in rainfall is characterized by adjustment to uniformly higher k_{sn} and an increase in steady state fluvial relief. For this model run, rainfall is decreased from 2 to 1 m/yr, causing discharge to decrease similarly by 50% (Movie S1).

We observe an effectively instantaneous transient decrease in erosion rate across the entire channel network driven by a decrease in erosional efficiency directly proportional in magnitude to the change (i.e., 50%; recall $m = 1$). The resulting disequilibrium, with $E < U$, drives surface uplift and upstream migration of a convex-up slope-break knickpoint, and eventually a ~40% increase in fluvial relief. This change in erosional efficiency differently affects k_{sn} and $k_{sn\text{-}q}$ (Figure 4).

In k_{sn}–E_{avg} space (Figure 4a), the change rainfall causes the trunk river and tributary network to shift uniformly onto a different erosional efficiency curve that describes the expected relationship between k_{sn} and erosion rate for a given erosional efficiency at steady state. Specifically, both shift from $K=2\cdot K_p$ to $K=K_p$ ($K_f = 0.5\cdot K_i$); thus, everywhere exhibits 50% lower erosional efficiency. Following this initial shift, the trunk river and individual tributaries approximately follow this new curve during adjustment toward higher erosion rates and k_{sn} to return to steady state, although in detail they deviate and exhibit a concave-

up trajectory. This deviation is a result of averaging segments above and below the migrating knickpoint into mean (upstream-averaged) k_{sn} and erosion rate values.

In $k_{sn\text{-}q}$–E_{avg} space (Figure 4b), both the initial and final steady state conditions plot in the same location on the curve for $K=K_p$. The initial decrease in erosional efficiency causes the trunk and tributaries to shift uniformly along this curve to lower $k_{sn\text{-}q}$ and erosion rate rather than shifting onto a different curve. During adjustment both generally follow this curve to return to steady state, minor transient deviations as seen for k_{sn} notwithstanding.

4.2 Case 2: Spatially Uniform Increase in Rainfall

The modelled catchment response to a spatially uniform increase in rainfall is characterized by adjustment to uniformly lower k_{sn} and a decrease in steady state fluvial relief. To compare responses, we invert the change in rainfall from the previous example, and rainfall is increased from 1 to 2 m/yr, which results in a 100% increase in discharge (Movie S2).

We observe a broadly symmetrical response to Case 1, where the twofold increase in rainfall leads to an initial twofold increase in erosion rate ($E > U$) and a ~30% decrease in steady state fluvial relief. The transient knickpoint is concave-up, but as it migrates upstream it relaxes and broadens, as is expected for a concave-up knickpoints where n > 1 (Royden & Perron, 2013). The signal of transient adjustment communicated to tributaries is consequently protracted, making morphological adjustments more diffuse in nature.

Responses reflected in k_{sn}–E_{avg} and $k_{sn\text{-}q}$–E_{avg} relationships also mirror Case 1. As is characteristic for k_{sn}, the initial change in erosional efficiency causes the trunk and tributary network to shift onto a different steady state erosional efficiency curve; in this case, from $K = K_p$ to $K = 2 \cdot K_p$, and they generally follow this curve during adjustment (Figure 4a). Minor deviations from this curve exhibit a convex-up pattern (inverted from Case 1) due to the opposite knickpoint shape in this case (concave vs. convex). Meanwhile in $k_{sn\text{-}q}$–E_{avg} space (Figure 4b), the initial and final steady state conditions for both the trunk and tributary network plot in the same location, as in Case 1. The change in rainfall again causes a shift only along the $K=K_p$ curve, but to uniformly higher $k_{sn\text{-}q}$ and erosion rate in this case, and they generally follow this curve during adjustment back to steady state.

4.3 Case 3: Spatially Uniform to Bottom-heavy (Overall Wetter Climate)

In this scenario, we model the catchment response to a change in rainfall pattern from spatially uniform

1.5 m/yr to a gradient that decreases upstream from 4 to 0.5 m/yr, which results a complex transient response. This change results in a nearly 80% increase in mean rainfall to ~2.7 m/yr, but also remarkably drives a 30% increase in fluvial relief (Figure 3b; Movie S3). Importantly, this contrasts with the 25% decrease in fluvial relief expected for a spatially uniform increase in mean rainfall of the same magnitude.

4.3.1 Case 3: Trunk Response

In this case, because the change in rainfall is variable along the trunk river, the initial change in erosion rate is also variable. The trunk river experiences an approximately 80% increase in erosion rate at the outlet ($E > U$), and a decrease of 67% in the headwaters ($E < U$), corresponding to the change in upstream average rainfall along its length. At x_{sc} (located ~27 km upstream from the outlet), $Q_f = Q_i$, $S_f = S_i$, and so immediately following the change in rainfall $E = U$ holds true; thus, no change in erosion rate occurs initially at x_{sc}. Increased erosion rate at the outlet produces a concave-up knickpoint; however, as the knickpoint migrates upstream it progressively sharpens and eventually evolves into an oversteepened convex-up knickpoint. Oversteepening is a consequence of the upstream decrease in erosional efficiency driven by the rainfall gradient that is exacerbated by, but does not depend on, differing modes of adjustment upstream and downstream of x_{sc} related to the complex response. This is analogous to knickpoint behavior described by Forte et al. (2016) and Darling et al. (2020) where modelled lithologic contacts demarcate similar relative variations in erosional efficiency (i.e. hard rocks over soft rocks). Lastly, we note that everywhere upstream of x_{sc} over-adjusts during transient adjustment leading to variable modes of adjustment in time as well as in space, which is a characteristic of complex responses in general. The overadjustment we observe is essentially the whiplash response described by Gasparini et al. (2006, 2007), but notably results here without sediment flux. This continuous evolution of the trunk knickpoint has important consequences for signals passed to tributaries.

4.3.2 Case 3: Tributary Response

Tributary responses to the change rainfall pattern depend largely on their position. Collectively, the network of tributaries experiences the full range of the rainfall gradient (i.e., 4 to 0.5 m/yr), and individual tributaries experience changes in erosional efficiency proportional to the change in rainfall that they experience. Notably, the change in rainfall and erosional efficiency experienced by a given tributary is always different from the trunk river at their confluence (Figure 2 inset). Additionally, tributaries also respond to changing boundary conditions related to continuous adjustment of the trunk river. These signals are often conflicting. For example, in this scenario, enhanced incision during the initial transient response of the trunk river causes tributaries in downstream locations ($x < x_{sc}$) to experience a relative

increase in the rate of base-level fall. Alone, this should promote profile steepening, but higher erosional efficiency due to higher rainfall in these tributaries counteracts steepening. The net effect of this competition plays out differently as a function of tributary position throughout the transient evolution (i.e., space and time) as 1) the discrepancy between the local rainfall conditions experienced by tributaries and the upstream averaged rainfall experienced by the trunk profile narrows upstream (Figure 2 inset), 2) the transient base level signal (i.e., trunk knickpoint) changes shape as it sweeps upstream, and 3) the duration of transient adjustment increases upstream.

4.3.3 Case 3: k_{sn}–E_{avg} and $k_{sn\text{-}q}$–E_{avg}

Plots of k_{sn}–E_{avg} and $k_{sn\text{-}q}$–E_{avg} clarify some additional features of the dynamic transient response to spatially variable rainfall as it sweeps through different parts of the catchment (Figure 5). We note that the trunk profile exhibits higher k_{sn} and $k_{sn\text{-}q}$ values and spans a relatively narrower range in erosion rates than tributaries during transient adjustment, reflecting the fundamentally different ways they experience the modelled rainfall gradient. This suggests that the network of tributaries (isolated smaller catchments that experience a range in rainfall) inherently incorporates a more direct signal of the change in rainfall patterns compared to the trunk, which averages upstream rainfall variations – an important finding for designing an effective sampling strategy in the field – discussed further in section 5.3.

In k_{sn}–E_{avg} space (Figures 5a, 5b), changes in erosional efficiency cause shifts onto curves for different erosional efficiencies, as in Cases 1 & 2, but notably different positions along the trunk river and individual tributary catchments shift by different amounts reflecting spatial variations in erosional efficiency. The trunk profile response spans curves for $K = 0.5 \cdot K_p$ to $\sim 1.8 \cdot K_p$, while the network of tributaries spans the range from curves for $K = 0.5 \cdot K_p$ to $4 \cdot K_p$. To first order, transient adjustment at a given location for the trunk, or of a given tributary, moves it along these different curves toward steady state as in Cases 1 & 2, but deviate in detail. As noted previously, positions upstream of x_{sc} over-adjust before returning to steady state, which affects these general trajectories more than for uniform changes in rainfall, exhibited by sharp inflections (Figure 5). Finally, we note that the final steady state condition for both the trunk profile and network of tributaries encompasses a range of erosion efficiency values (Figures 5a & 5b). Interestingly, for the trunk profile, the range of erosional efficiency values that correspond to upstream mean k_{sn} values at steady state ($K = 0.5 \cdot K_p$ to $\sim 1.8 \cdot K_p$) are lower than that implied by mean rainfall (i.e., $K = \sim 2.7 \cdot K_p$; Figures 1b, 5a) – discussed further in section 5.2.

In $k_{sn\text{-}q}$–E_{avg} space (Figures 5c, 5d), differences between trunk and tributary responses and important differences from k_{sn} are readily apparent. Initial and final steady state conditions plot in the same position,

as is characteristic of $k_{sn\text{-}q}$ because uplift rate is constant. Following the change in rainfall, the trunk profile expands subparallel to the $K=K_p$ curve, where downstream locations are systematically shifted toward higher erosional efficiency. This shift reflects systematic slope adjustments that must occur along the trunk to bring it into equilibrium with the non-uniform rainfall pattern, and decreases with time as morphological adjustments take place. Apart from this minor shift, different positions along the trunk profile generally follow the $K=K_p$ curve during adjustment back to steady state. In tributaries, on the other hand, the change in rainfall causes expansion precisely along the $K=K_p$ curve because they experience no along-stream variations in rainfall. Tributaries again generally evolve along the $K=K_p$ curve toward steady state (as with cases 1 and 2). Transient morphological adjustments affect this trajectory in detail and deviations, which affect apparent erosional efficiency, are more significant in drier tributaries near the headwaters. Overadjustment is also evident for both the trunk and tributaries, but because transient evolution is generally along the steady state curve, it does not significantly affect the apparent erosional efficiency. As a final note, we point out that dispersion around steady state erosional efficiency curve in $k_{sn\text{-}q}$–E_{avg} space is minor over the entire course of the transient adjustment compared to dispersion in k_{sn}–E_{avg} space – we expand on implications from this point in section 5.3.

4.4 Case 4: Spatially Uniform to Top-heavy (Overall Drier Climate)

In this final case, we the model the catchment response to a change in rainfall pattern from spatially uniform 1.5 m/yr to a gradient that increases upstream from 0.25 to 2.25 m/yr, which also results a complex transient response. This change results in a decrease in mean rainfall by 33% and a 10% decrease in fluvial relief (Figure 3; Movie S4). Notably, this contrasts with a 22% increase in fluvial relief that would be expected for a spatially uniform decrease in mean rainfall of the same magnitude.

4.4.1 Case 4: Trunk Response

In this case, the trunk river experiences a 33% initial decrease in erosional efficiency and erosion rate at the outlet, and a 50% increase in the headwaters immediately following the change in rainfall pattern (Figure 6). However, we note that this range is significantly narrower than the range of variations in rainfall because of the buffering effect that concentrating rainfall in the headwaters has on downstream changes in discharge (e.g., Figure 2 inset). Like Case 3, because this scenario also exhibits a complex transient response, the transition between decreases in erosion rate downstream and increases upstream is initially at position x_{sc}. Unlike Case 3, knickpoint shape does not invert during transient adjustment and is always convex-up, although it does tend to relax downstream and sharpen upstream from x_{sc}, respectively. Retention of the knickpoint shape is accommodated by over-adjustment upstream of x_{sc}, specifically by

progressively more rapid upstream adjustment (higher erosional efficiency) toward gentler slopes that outpaces downstream adjustment. Because $E > U$ upstream of x_{sc}, over-adjustment of the profile promotes incision below its steady state elevation and always adjusts to steady state from an understeepened condition. Therefore, by the time that the migrating trunk knickpoint reaches positions upstream of x_{sc}, the channel bed must uplift and the profile must steepen to achieve steady state, preserving the convex-up knickpoint shape (Movie S4).

4.4.2 Case 4 Tributary Response

Complexities in the trunk response again dramatically affect the tributary responses, and generally mirror complexities discussed in Case 3. Tributaries again respond to variable, and commonly, conflicting signals. In this case, downstream of x_{sc}, tributaries initially respond to a decrease in rainfall (lower - erosional efficiency) by steepening. However, along that same region the trunk profile experiences a decrease in erosional efficiency that drives steepening and surface uplift, forcing tributaries to respond to a conflicting signal of base-level rise (Movie S4). Additionally, as the network of tributaries experiences the full range of the rainfall gradient – thus express a broader range in erosional efficiency – individual tributaries in downstream locations are relatively much drier and adjust relatively slowly compared to upstream locations. Interestingly, the trunk profile adjusts and communicates transient base-level signals upstream to wetter tributaries relatively quickly compared to the adjustment timescale of these dry tributaries, which follows as the trunk has much higher erosional efficiency from rainfall in its headwaters. The initially counterintuitive result of this is that central portions of the catchment are the first to achieve steady state (i.e., both the trunk profile and tributaries achieve the new steady state), followed by the headwaters, and lastly tributaries near the outlet where the transient signal originated.

4.3.3 Case 4: k_{sn}–E_{avg} and $k_{sn\text{-}q}$–E_{avg}

Evolution of k_{sn}–E_{avg} and $k_{sn\text{-}q}$–E_{avg} relationships during the transient evolution are generally similar to Case 3, but a few aspects are notably different. First, the disparity between final steady state conditions for the trunk profile and network of tributaries is significantly greater than Case 3 (Figures 6a, 6b), which reflects the extent to which variations in erosional efficiency are buffered along the trunk profile by concentrating rainfall near the headwaters. We also note that in $k_{sn\text{-}q}$–E_{avg} space, apparent erosional efficiency is more strongly affected during transient adjustment in the tributary network compared to the trunk profile (transient deviations from the K=K_p curve), but also compared to Case 3. Large deviations are again restricted to drier tributary catchments, and comparison to Case 3 expresses that changes in rainfall have a non-linear effect (Equations 1,7). That said, even these stronger effects on apparent

erosional efficiency in $k_{sn\text{-}q}$–E_{avg} space are still minor compared to representing any equivalent time in the k_{sn}–E_{avg} relationship with a single erosional efficiency (K) value. Finally, also like Case 3, the range of erosional efficiency values for the trunk profile (K = ~1.8·K_p to 2.25·K_p) are different, in this case higher, than is implied by mean rainfall (i.e., K = ~K_p; Figures 1b, 6a) – discussed further in section 5.2.

5. Discussion

The central themes we have explored so far are how the spatial rainfall pattern influences the channel profile morphology, and how temporal changes in rainfall pattern affect erosion rates and profile morphology during periods of transient adjustment. We have detailed the expected response to along-stream variations in erosional efficiency caused by spatial rainfall gradients according to the SPM and have shown how the transient response to a change in rainfall pattern is fundamentally different from a spatially uniform change in rainfall. A change in rainfall pattern will always result in spatio-temporally variable changes in erosion rates, which in some circumstances means a given location may over time experience both elevated and reduced erosion rates and channel steepness values relative to equilibrium in response to a single change in rainfall. It is important to keep in mind, however, that the nature of transient response depends strongly on the initial equilibrium conditions at the time of the change in rainfall pattern. Therefore, there is a complex relationship between the transient response at any given location or time and both the change in mean rainfall and the final rainfall pattern. In the following discussion, we focus on highlighting some implications for the different expectations that follow from changes in rainfall pattern. Specifically, we show some examples where conventional expectations based on spatially uniform changes in rainfall can lead researchers astray, and where possible, we attempt to identify additional information or strategies that may be leveraged by future studies to overcome these challenges.

5.1 Revising Expectations for Erosional and Morphological Responses to Changing Climate

5.1.1 Relative Nature of Erosional Response

To this point, our choice of a steady state initial condition with spatially uniform rainfall has been convenient, as have been the terms top-heavy and bottom-heavy to describe typical rainfall patterns. While idealized, this provides an intuitive starting point for understanding how more complicated – but almost certainly more realistic – climate change scenarios might play out. Recall, according to the SPM, transient climate-driven changes in erosion rate are dictated by a *relative* change in discharge. Where discharge is increased, erosion rates increase in response and river gradient declines toward a new equilibrium steepness; thus, a river subjected to an increase in discharge can be considered locally, if

transiently, oversteepened relative to equilibrium, and vice versa. As we have shown, because discharge generally accumulates non-linearly downstream within a river basin, a change in rainfall pattern can readily create circumstances where the relative change in discharge inverts along the river length – at position x_{sc} (Figure 2) – producing a complex transient response (Figures 2 & 3). Importantly, inversion along the profile implies that the river is simultaneously oversteepened and understeepened on either side of position x_{sc}, and these transient states dictate whether erosion rates initially increase or decrease following the change in rainfall, respectively, not whether the new rainfall pattern is itself top-heavy or bottom-heavy. The positions of these transient states then shift throughout adjustment.

The nature of landscape response to relative changes in discharge implies, for instance, that relaxation of a bottom-heavy rainfall gradient can cause a complex transient response resembling a change from uniform to top-heavy rainfall patterns. That is, a gentler bottom-heavy gradient is relatively top-heavy compared to an extreme bottom-heavy gradient; similarly, a gentler top-heavy gradient is relatively bottom-heavy compared to an extreme top-heavy gradient, and vice versa (Figure 7). Thus, for a change in climate that causes an extreme bottom-heavy rainfall gradient to relax *and* results in a complex transient response (e.g., Figure 7a), rainfall and erosion rate are expected to increase in the headwaters of the catchment and decrease near the outlet. While the rainfall pattern is always bottom-heavy, this expected erosional response is like the change from uniform to a top-heavy rainfall pattern described in Case 4. This response, however, is not consistent with expectations for any uniform increase or decrease in rainfall, even if such a shift accurately reflects the change in mean rainfall and rainfall pattern. Therefore, neither the final rainfall pattern alone nor the relative change in mean rainfall (wetter or drier) allow a robust prediction of changes in erosion rate within a catchment following a regional change in climate.

Interestingly, changes in climate do not need to involve extreme changes in rainfall patterns (e.g., reversal from top-heavy to bottom-heavy) to drive complex transient responses. Instead, a wide range of changes to orographic patterns, including relatively subtle variations, that may reasonably be expected in response to global climate changes, may significantly, if temporarily, alter the spatial pattern of erosion in a given river basin. Because such complex, climate change-driven patterns of erosion are not reasonably captured by a conceptual framework based on spatially uniform changes in rainfall, as documented above (compare Cases 3 & 4 to Cases 1 & 2), apparent inconsistencies between expectations and observations have the potential to give a false impression about the primary forcing(s) controlling erosion rates.

5.1.2 Multi-stage Adjustment

It has long been recognized that spatially uniform changes in rainfall should promote transient changes erosion rate everywhere across a landscape, which causes morphological adjustments to sweep upstream as erosional equilibrium is restored (e.g., Tucker & Slingerland, 1997; Whipple & Tucker, 1999). Our model is fully consistent with this expectation under such conditions (e.g., Cases 1 & 2). In addition, we have shown that responses to changes in the rainfall pattern are variable in both space and time (e.g., Cases 3 & 4). An important consequence of this is that following any non-uniform change in rainfall pattern, distinct initial morphological and erosional changes always precede the upstream sweeping adjustments that ultimately restore equilibrium. Thus, contrary to expectations for a uniform change in rainfall, we find that catchments characteristically exhibit a relatively protracted, multi-stage, and spatio-temporally variable response to a single change in rainfall pattern (Figure 8; Movie S5). We emphasize that this behavior is a general characteristic of any non-uniform change in rainfall pattern and is not exclusive to those that induce the complex transient responses. This leads to novel expectations for how transient responses to changes in climate should be expressed across a landscape and has potentially important implications for detecting transient landscape responses to climate changes.

The initial stage of morphological adjustment begins synchronously across the entire river basin following a change in rainfall pattern. At the onset, local erosion rate is everywhere a function of the local relative change in discharge for both trunk and tributary profiles, as described in Cases 3 & 4. As this initial stage proceeds, spatial variations in erosion rate along the trunk river produce morphological changes along its entire length that progress at different rates (variable erosional efficiency). Importantly, this means that initial, or "relict", conditions are often not preserved upstream of slope-break knickpoints on the trunk profile; the profile is progressively modified as adjustment proceeds even upstream of the main knickpoint. Indeed, the resemblance of "unadjusted" profile segments upstream from the main knickpoint to their initial state diminishes with time during the transient response, and thus with relative position upstream. This contrasts with spatially uniform changes in rainfall (and erosional efficiency), or uplift rate that does not affect erosional efficiency, that allow preservation of relict morphological characteristics (e.g., k_{sn}) upstream of migrating transient knickpoints, as is often assumed in analysis and inversions of river profiles (e.g., Clark et al., 2006; Fox et al., 2014; Gallen et al., 2013; Goren et al., 2014; Kirby & Whipple, 2012; Miller et al., 2013; Schoenbohm et al., 2004; Whittaker et al., 2007). More broadly, this contrasts with the notion that climate change should simply propagate upstream from base level as is expected for other external changes (e.g., uplift rate). While there is a signal of transient adjustment that indeed migrates upstream, significant amounts of surface uplift, as observed in Case 3 (Movie S3), or incision, as observed in Case 4 (Movie S4), along with changes in channel steepness can occur prior to arrival of this signal. Nevertheless, these changes are in response to the change in climate.

Additionally, spatio-temporally variable adjustments along the trunk profile dictate that individual tributaries experience temporally variable rates of base-level fall until the trunk profile reaches a new equilibrium at their confluence (Movie S3 & S4).

The continuous, yet variable nature of base-level fall imposed by the trunk river on tributaries during the initial stage of adjustment generally results in a broad adjustment zone characterized by smooth variations in channel steepness in tributary catchments. Indeed, tributaries in our model located in upstream positions where this initial adjustment stage is relatively long-lived (compared to tributaries located near the trunk outlet) experience significant changes in slope and relief without formation of any knickpoints (e.g., Figure 8b; Movies S3 & S4). Importantly, this shows that tributaries are not insulated from effects of spatially variable changes in rainfall (variable erosional efficiency) along their trunk river, even if they experience essentially uniform rainfall throughout their history. Furthermore, they may appear relatively well-adjusted (graded) during periods of transient adjustment despite significant deviation from both initial and final steady state conditions (Figure 8b; also see Tributary 2, Movies S3 & S4).

Adjustment to quasi-steady-state conditions along the trunk river, which may or may not be associated with the upstream migration of a significant or obvious slope-break knickpoint, defines the beginning of the second – and final – stage of adjustment in our model landscapes (Figure 8). The rate of base-level fall experienced by a given tributary stabilizes upon local adjustment of the trunk profile, representing a distinct change from the initial stage where the rate of base-level fall is temporally variable. Depending on circumstances, this change may be abrupt and produce a discrete knickpoint that sweeps upstream through the tributary catchment. The change in base-level fall rate is the dominant signal exhibited during this second adjustment stage, although it acts upon the profile state reached during the initial adjustment stage, and it is largely a function of the shape and migration rate of the trunk knickpoint. Both factors are controlled by the integrated response of the trunk profile to this point, and therefore do not relate to the change in rainfall pattern in a direct manner. Therefore, importantly, the dominant signal passed to tributaries during this second stage, and any knickpoints that form as a result, generally do not reflect the change in rainfall locally within the tributary catchment, and their relationship to the regional rainfall pattern experienced by the trunk stream is complex. This is directly contrary to expectations for spatially uniform changes in rainfall where changes in slope above and below knickpoints should scale with the magnitude of the change in rainfall (e.g., Whipple, 2001).

Extrapolating these observations to natural, inherently more complex trellised river networks, suggests that broad adjustment zones comprising multiple knickpoints might be associated with a given change in rainfall pattern – in contrast to the single knickpoint or knickzone expected to accompany a spatially

uniform change in rainfall magnitude (e.g., Case 1 & 2). For instance, if second-order rivers (*sensu* Hack, 1957) experience spatially variable rainfall patterns in addition to the trunk, then we expect third-order rivers should experience an additional pair of adjustment stages. Importantly, this analysis implies that the full transient response to changes in rainfall pattern may be expressed in a complex fashion, and potentially across a large areal extent, in large river basins (e.g., Figure 8; Movie S5). If true, this multi-stage adjustment behavior may ultimately pose a significant, still unresolved, challenge to recognizing and quantifying transient responses to changes in climate in many settings.

5.2 The Influence of Climate on Topography and Erosion Rates

5.2.1 Steady State Relationships among Channel Steepness, Erosion Rate, and Erosional Efficiency

The SPM makes specific predictions about the relationships among channel steepness, erosion rate, and erosional efficiency (K) at steady state, as stated by Equations 7a & 7b and shown by curves in Figures 4-6. Because the role of climate is encapsulated in K, it is important to remember that a uniform K value implies that the influence of climate is uniform over the spatial and temporal scales of interest. Further, the expectation that basin-average topographic metrics like k_{sn} should relate to rainfall in a simple way generally relies on an assumption of a spatially uniform K value. Rainfall gradients systematically affect this expectation, where bottom-heavy gradients result in higher k_{sn} (lower apparent erosional efficiency), while top-heavy gradients result in lower k_{sn} (higher apparent erosional efficiency) (Figure 9). The magnitude of this effect (as a percentage of actual erosional efficiency) varies with strength of the rainfall gradient, but importantly, k_{sn} values also vary with uplift rate (Equation 7a). Therefore, while subtle rainfall gradients affect apparent erosional efficiency to a proportionally lesser degree, they can still substantially influence observed k_{sn} values where uplift rates are higher. This can be important in natural settings where uplift rates, erosional efficiency, and the form of their relationship to topography are generally unknown.

This analysis has two related, and important implications. First, interpretation of the controls on topography (e.g., mean k_{sn}, mean gradient, relief, etc.) in terms of climate sensitivity, uplift, and/or rock properties using measurements from catchments that experience the same mean rainfall, but different rainfall patterns, is not necessarily valid even at steady state. Second, it predicts weaker correlations (more dispersed) between topographic metrics and erosion rate than would be expected if rainfall were always uniformly distributed, as is implied by use of basin-average rainfall (Figure 9). This prediction applies even before considering any geologic uncertainties (e.g., at quasi-steady-state or potentially transient?), analytical uncertainty, and even if no other variations in K exist. Because rainfall gradients create systematic, rather than random, dispersion around relationships expected for uniformly distributed

rainfall, there is not necessarily any expectation that larger datasets will more accurately resolve variations in erosional efficiency unless catchments where rainfall is uniform and are isolated, or a correction is made for the influence of spatially variable rainfall (e.g., using $k_{sn\text{-}q}$). Rather, compilation of topographic measurements from basins that do and do not experience rainfall gradients can, in and of itself, obscure or, depending on circumstances, distort the actual influence of rainfall on erosional efficiency (Figure 9). This result is of particular importance for designing future efforts to empirically test the SPM in natural settings.

5.2.2 Misleading Transient Signals

Spatial patterns in erosion rate are commonly used to inform tectonic models and to infer rock uplift rates in mountain landscapes (e.g., Adams et al., 2020; Godard et al., 2014; Kober et al., 2015; Morell et al., 2015; Safran et al., 2005; Scherler et al., 2014). However, we have shown that changes in rainfall patterns can drive long-lived and complex spatial patterns of erosion that differ from expectations for uniform changes in rainfall (Whipple, 2001; Whipple & Tucker, 1999) and thus may not be readily recognized and interpreted. We have also shown that that ongoing transient adjustment may not be obviously expressed in landscape morphology (especially for catchment-mean metrics) under some circumstances. If these caveats are not considered, subtly expressed transient spatial variations in erosion rate may be mistaken as representing quasi-steady state spatial variations in uplift rate (i.e., $E = U$). At once this would give a false impression about the spatial pattern of uplift and about the importance of past climate changes on landscape evolution, with direct implications for understanding connections among climate, surface processes, and tectonics. Determining whether there are circumstances in which spatial patterns of erosion and topography produced by changes in rainfall patterns can be misleading enough to confound interpretations is therefore critically important.

During the early transient adjustment in Case 3 (transition to a bottom-heavy rainfall pattern) there is a clear example of circumstances where such confusion may occur (Figure 10). Recall, in this case, early transient adjustment produces a concave-up knickpoint along the trunk profile but as it migrates upstream the shape evolves. This creates a broad adjustment zone. Over the first ~500 kyr, quasi-steady state adjustment proceeds ~60% upstream along the trunk, but the broad adjustment zone means most tributaries along this length experience a protracted signal of base-level changes related to trunk adjustment. Because these tributaries all also experience a net increase in rainfall, knickpoints associated with local adjustment of the trunk river (Stage 2) tend to relax as they work upstream making them more diffuse. This protracted competition between local rainfall and spatio-temporally variable rates of base-level fall, generally results in diffuse concave to broad convexo-concave adjustment zones in tributaries

(e.g., Figure 8a; Movie S5). Broad adjustment zones, particularly concave-up adjustment zones, are inherently subtle and this can inhibit their recognition. This problem may be further compounded by the influence of sediment flux in natural settings (Brocard & Van Der Beek, 2006; Whipple & Tucker, 2002). Indeed, even in our idealized model (i.e., no sediment influence), along-stream variations in trunk and tributary local k_{sn} variation is diffuse (Figure 10c). Based on a lack of significant knickpoints that might indicate transient adjustment and the several-fold spatial variation in erosion rate, one might reasonably interpret relationships depicted in Figure 10a reflect a quasi-steady-state landscape adjusted to a spatial gradient in uplift rate. In the absence of a surface breaking structures that might accommodate this gradient in uplift, blind structures may be inferred, with potential implications for tectonic models. The apparent viability of this interpretation is supported by the SPM if rock uplift rate is assumed to match the observed pattern of catchment averaged erosion rates in tributaries (steady-state conditions) as illustrated in Figure 10b. Figure 10b shows that the predicted steady-state upstream-averaged k_{sn} pattern along the trunk river and mean k_{sn} values exhibited by the tributary network is essentially identical to the transient pattern in Figure 10a. Moreover, even in detail, there are only subtle differences in the along-stream pattern of local k_{sn} between the two scenarios (Figure 10c). Thus, in this instance, k_{sn} patterns and erosion rates that actually record a complex transient response to a change in rainfall pattern could reasonably be mistaken for a steady state landscape adjusted to a spatial gradient in uplift.

Importantly, we note that for this example the spatial pattern of $k_{sn\text{-}q}$ unambiguously suggests along-stream variations in erosion rate exist along both the trunk river and tributaries. It also exhibits a coherent pattern of downstream adjustment that could readily be interpreted as a transient signal sweeping upstream through the catchment that, significantly, is inconsistent with a steady state landscape adjusted to the spatial gradient in uplift shown in Figure 10b (Figure 10c). This example shows the potential usefulness of $k_{sn\text{-}q}$, both as a diagnostic tool for detecting ongoing transient adjustment to changes in rainfall patterns where k_{sn} may be misleading and for resolving the relative influences of tectonics and climate.

Finally, we emphasize that our intention is not to suggest all, or any specific examples, where spatial patterns of rock uplift are inferred from erosion rates and channel steepness patterns are incorrect. Rather, our intention here is to highlight the extent to which confusion may be possible under the right circumstances, and how explicitly accounting for rainfall patterns can be a step toward addressing these challenges.

5.3 Toward Detecting the Influence of Climate on Topography and Erosion Rates

As our various examples have shown, remote analysis of channel steepness patterns can provide a

preliminary means to detect whether spatial variations in rainfall may be influencing river profiles in a landscape, and whether transient adjustment to a change in rainfall pattern may be ongoing. For landscapes well-described by the SPM, discrepancies between rainfall conditions experienced by trunk and tributary basins should cause systematic differences in trunk and tributary k_{sn} (Figures 5&6; Gasparini & Whipple, 2014), but not in $k_{sn\text{-}q}$. As illustrated in Figure 10c, the expected contrast in trunk and tributary k_{sn} is most developed at steady state, but it begins manifesting immediately during transient adjustment as differences in local k_{sn} at confluences that migrate upstream (Figure 10c, Movie S5). In contrast, precise agreement between trunk and tributary $k_{sn\text{-}q}$ is expected at steady state, and it is approximately maintained even during periods of adjustment to a change in rainfall pattern. In addition, we note that agreement between trunk and tributary $k_{sn\text{-}q}$ that weakens upstream from confluences may be an important indication of ongoing transient adjustment that may be difficult detect from the k_{sn} pattern alone (Figure 10c, e.g., as discussed in section 5.2.2). Therefore, comparison of k_{sn} and $k_{sn\text{-}q}$ patterns may at once be a potentially useful way to diagnose and further assess the potential extent of influence by rainfall gradients, provided the pattern of discharge accumulation can be reasonably estimated (e.g., using high spatial resolution satellite rainfall or nested stream gauge data).

Following topographic analysis, our results have additional implications for designing effective catchment-averaged erosion rate sampling strategies. Broadly, sampling strategies can be grouped into two classes: nested and distributed, described below. Nested, or hierarchical, sampling strategies comprise multiple samples from the same river basin where some or all samples are collected along the trunk river, and where averages typically integrate over very large (10^2–10^5 km^2) drainage areas (e.g., Abbühl et al., 2010; Henck et al., 2011; Portenga et al., 2015; Reinhardt et al., 2007; Safran et al., 2005; Willenbring et al., 2013). In principle, such strategies can allow researchers to assess reproducibility of individual measurements, test sediment mixing models, and sub-divide basins into different sectors to identify along-stream variations in erosion rates. Given the complex along-stream patterns of erosion rate we observe in response to changing rainfall patterns and widely disparate responses between trunk and tributary profiles, however, our results suggest that caution is warranted in interpreting patterns of erosion rates collected in a nested fashion. In particular, this includes datasets that compile measurements from along trunk rivers and tributary catchments, but also those that compare samples from different large catchments that experience different mean climates and rainfall patterns, even at quasi-steady-state, because how each reflects and experiences variations in rainfall may be fundamentally different. Furthermore, because we find that along-stream variations in erosion rate due to changes in rainfall pattern are characteristically muted along the trunk profile (e.g., Figure 10a), nested strategies may not be appropriate in many settings, especially if the goal is to measure the influence of climate on fluvial

incision.

The other widely used strategy, which we refer to as a distributed sampling strategy, targets single samples from catchments that are distributed across a landscape or mountain front, and typically – though certainly not always – comprises relatively smaller (10^0-10^2 km^2) catchments (e.g., Adams et al., 2020; Binnie et al., 2008; Carretier et al., 2013; DiBiase et al., 2010; Godard et al., 2014; Morell et al., 2015; Ouimet et al., 2009; Scherler et al., 2014). This type of strategy generally allows more freedom to carefully select preferable catchments (relatively uniform channel steepness, rainfall, lithology), with the limitation that spatial variations in erosion at the sub-catchment scale are not resolvable with single measurements. As a counter point to muted spatial variations in erosion noted for nested strategies, our model results suggest this type of strategy inherently records a more direct signal of any climatic influence. However, if inter-catchment variations in rainfall and therefore erosional efficiency are not accounted for, or transient conditions are not recognized, this sensitivity may cause significant dispersion or distortion in relationships among landscape metrics, as shown for k_{sn}–E_{avg} relationships (Figures 5b & 6b), and/or lead to misleading spatial patterns in erosion and channel steepness (Figure 10).

Lastly, we note that transient adjustments in response to changes in rainfall pattern do not significantly affect apparent erosional efficiency in $k_{sn\text{-}q}$–E_{avg} relationships where no variations in rock properties exist, even in response to the dramatic shifts in rainfall patterns that we model, regardless of sampling strategy. Indeed, transient deviations from expected steady state relationships modelled in any location are generally well within the analytical uncertainty of measured catchment-average erosion rates from natural landscapes (Figures 5 and 6). Exceptions to this appear to be limited to scenarios where landscapes experience a shift toward arid climates. Nevertheless, transient, spatially variable patterns of erosion due to changes in rainfall pattern are reflected in $k_{sn\text{-}q}$ patterns with good accuracy in our model (Figure 10c, Movie S3-S5), and thus $k_{sn\text{-}q}$ may be used to recognize ongoing adjustment to changes in climate where k_{sn} can be ambiguous. Therefore, we suggest that $k_{sn\text{-}q}$, or a different metric that encompasses the spatial distribution of rainfall (runoff), may be vital component for future efforts to detect climate's influence on and from topography and erosion rates in mountain landscapes where rainfall is inherently spatially variable.

5.4 Caveats and Limitations

Here we emphasize several important caveats should be kept in mind when evaluating the results and subsequent discussion presented here. First, and foremost, our modelling efforts explicitly assume that landscapes are inherently sensitive to climate (through rainfall) in a manner described by the SPM. While

788 the intuitive support for such sensitivity is strong, and evidence from natural landscapes is mounting that
789 broadly support predictions of the SPM (e.g., Adams, et al., 2020; Harel et al., 2016; Lague, 2014), there
790 remains a large amount of uncertainty about the strength of the sensitivity to climate.

791 Following the core assumption that the SPM is broadly applicable, we note that our model setup is very
792 simple. We assume that all precipitation is rainfall, all rainfall is converted directly to runoff, and we
793 impose constant rainfall gradients that act precisely along the trunk stream and basin axis and that span
794 the entire length of our modelled river basin. While some river basins set within mountain-belt scale
795 orographic precipitation patterns may indeed experience rainfall patterns consistent with this simple
796 geometry, we note that non-linear, and even non-monotonic, rainfall gradients are common for large river
797 basins or those characterized by high local relief (Roe, 2005). In addition, we model tributary catchments
798 that are uniform in size that experience uniform rainfall. Preliminary model investigations suggest that
799 although allowing tributary sizes and rainfall to vary causes some dispersion in the relationships
800 illustrated here, the overall behavior we describe remains the dominant signal. Nevertheless, both aspects
801 warrant further investigation.

802 Lastly, we emphasize that we use a simple version of the SPM where, among other simplifications, we
803 treat erosion exclusively as detachment limited. While assuming detachment-limited conditions is
804 common, particularly for describing erosion in mountain settings, it may not always be appropriate even
805 in these settings to describe transient behavior (Whipple & Tucker, 2002). Related to this, our treatment
806 of K_p, while incrementally more complex than spatially uniform erosional efficiency, remains highly
807 simplified. We do not explore the myriad of other factors that control erosional efficiency (K), and the
808 likelihood that rainfall, or more broadly climate, will influence rock erodibility ($\sim K_p$) and size distribution
809 of sediment delivered to rivers (Ferrier et al., 2013; Murphy et al., 2016; Neely & DiBiase, 2020; Riebe et
810 al., 2015; Sklar et al., 2017).

811 **6. Summary and Conclusions**

812 In this study, we use a simple form of the SPM to explore how spatial rainfall gradients influence both
813 river profiles and expectations about how fluvial landscapes should respond to changes in climate.
814 Notably, because changes in climate in mountain settings are likely to involve changes in precipitation
815 patterns, we expect that advancing understanding about how changes in climate influence the relief and
816 topographic form of mountain landscapes requires a more nuanced, spatially variable, treatment of
817 climate at the catchment scale beyond broadly characterized changes in mean climate. We show that
818 spatially varying rainfall conditions experienced by rivers occupying different landscape positions,

specifically trunk and tributary rivers, result in fundamentally different expressions of a given rainfall pattern, and that they respond to changes in rainfall pattern in fundamentally different ways. Further, we show how the non-linear nature discharge accumulation in a catchment means that even modest variations in rainfall patterns can result in significant changes to spatial patterns of erosion and topography that directly contrast with expectations for uniform changes in rainfall. In particular, changes in rainfall pattern characteristically result in multi-stage responses with adjustment zones that can be both spatially extensive and subtly expressed, thus difficult to recognize. Interestingly, these finding suggest more broadly that catchments of different sizes, shapes, and locations set within regional orographic precipitation patterns may have unique, and substantially variable, rainfall histories and responses to changes in climate. These complications raise important questions about how best to interpret spatial variations in erosion rates and their relation with topography, particularly from along-strike of orogenic fronts where different transverse rivers may record broadly similar forcing in fundamentally different ways. Finally, we show how catchment-scale variations in rainfall generally complicate relationships between conventional topographic metrics (e.g., mean k_{sn}) and erosion rates, even at steady state, which has implications for empirical tests of the SPM in natural landscapes. More precise metrics like $k_{sn\text{-}q}$ that leverage ever-increasing resolution of rainfall datasets to better account for the spatial distribution of rainfall – specifically its effect on discharge and runoff – may be a significant step toward overcoming these challenges, and may prove vital for future studies seeking to quantify interactions between climate, tectonics, and erosion in mountain landscapes.

Acknowledgments

This manuscript has benefitted from many insightful discussions over the years. Funding for this project was provided by the Tectonics program at NSF (EAR-1842065 to K.X.W.). Supplementary movies will be uploaded with this manuscript, and model is described in detail in main text. No data were used, nor created for this research.

References

Abbühl, L. M., Norton, K. P., Schlunegger, F., Kracht, O., Aldahan, A., & Possnert, G. (2010). El Niño forcing on 10Be-based surface denudation rates in the northwestern Peruvian Andes? *Geomorphology*, *123*(3–4), 257–268. https://doi.org/10.1016/j.geomorph.2010.07.017

Adams, B. A., Whipple, K. X., Forte, A. M., Heimsath, A. M., & Hodges, K. V. (2020). Climate controls on erosion in tectonically active landscapes. *Science Advances*, *6*(42), eaaz3166. https://doi.org/10.1126/sciadv.aaz3166

Bierman, P., & Steig, E. J. (1996). Estimating Rates of Denudation Using Cosmogenic Isotope Abundances in Sediment. *Earth Surface Processes and Landforms*, *21*(2), 125–139. https://doi.org/10.1002/(sici)1096-9837(199602)21:2<125::aid-esp511>3.0.co;2-8

Binnie, S. A., Phillips, W. M., Summerfield, M. A., Fifield, L. K., & Spotila, J. A. (2008). Patterns of denudation through time in the San Bernardino Mountains, California: Implications for early-stage orogenesis. *Earth and Planetary Science Letters*, *276*(1–2), 62–72. https://doi.org/10.1016/j.epsl.2008.09.008

Bonnet, S., & Crave, A. (2003). Landscape response to climate change: Insights from experimental modeling and implications for tectonic versus climatic uplift of topography. *Geology*, *31*(2), 123–126. https://doi.org/10.1130/0091-7613(2003)031<0123:LRTCCI>2.0.CO;2

Bookhagen, B., & Strecker, M. R. (2012). Spatiotemporal trends in erosion rates across a pronounced rainfall gradient: Examples from the southern Central Andes. *Earth and Planetary Science Letters*, *327–328*, 97–110. https://doi.org/10.1016/j.epsl.2012.02.005

Brocard, G. Y., & Van Der Beek, P. A. (2006). Influence of incision rate, rock strength, and bedload supply on bedrock river gradients and valley-flat widths: Field-based evidence and calibrations from western Alpine rivers (southeast France). *Special Paper of the Geological Society of America*, *398*, 101–126. https://doi.org/10.1130/2006.2398(07)

Brown, E. T., Stallard, R. F., Larsen, M. C., Raisbeck, G. M., & Yiou, F. (1995). Denudation rates determined from the accumulation of in situ-produced 10Be in the luquillo experimental forest, Puerto Rico. *Earth and Planetary Science Letters*, *129*(1–4), 193–202. https://doi.org/10.1016/0012-821X(94)00249-X

Carretier, S., Regard, V., Vassallo, R., Aguilar, G., Martinod, J., Riquelme, R., et al. (2013). Slope and climate variability control of erosion in the Andes of central Chile. *Geology*, *41*(2), 195–198. https://doi.org/10.1130/G33735.1

Clark, M. K., Royden, L. H., Whipple, K. X., Burchfiel, B. C., Zhang, X., & Tang, W. (2006). Use of a regional, relict landscape to measure vertical deformation of the eastern Tibetan Plateau. *Journal of Geophysical Research: Earth Surface*, *111*(3), 1–23. https://doi.org/10.1029/2005JF000294

Cyr, A. J., Granger, D. E., Olivetti, V., & Molin, P. (2014). Distinguishing between tectonic and lithologic controls on bedrock channel longitudinal profiles using cosmogenic 10Be erosion rates and channel steepness index. *Geomorphology*, *209*, 27–38. https://doi.org/10.1016/j.geomorph.2013.12.010

D'Arcy, M., & Whittaker, A. C. (2014). Geomorphic constraints on landscape sensitivity to climate in tectonically active areas. *Geomorphology*, *204*, 366–381. https://doi.org/10.1016/j.geomorph.2013.08.019

Darling, A., Whipple, K., Bierman, P., Clarke, B., & Heimsath, A. (2020). Resistant rock layers amplify cosmogenically-determined erosion rates. *Earth Surface Processes and Landforms*, *45*(2), 312–330. https://doi.org/10.1002/esp.4730

DiBiase, R. A., Whipple, K. X., Heimsath, A. M., & Ouimet, W. B. (2010). Landscape form and millennial erosion rates in the San Gabriel Mountains, CA. *Earth and Planetary Science Letters*, *289*(1–2), 134–144. https://doi.org/10.1016/j.epsl.2009.10.036

Duvall, A. (2004). Tectonic and lithologic controls on bedrock channel profiles and processes in coastal California. *Journal of Geophysical Research*, *109*(F3), 1–18. https://doi.org/10.1029/2003jf000086

Ferrier, K. L., Huppert, K. L., & Perron, J. T. (2013). Climatic control of bedrock river incision. *Nature*, *496*(7444), 206–209. https://doi.org/10.1038/nature11982

Forte, A. M., Yanites, B. J., & Whipple, K. X. (2016). Complexities of landscape evolution during incision through layered stratigraphy with contrasts in rock strength. *Earth Surface Processes and Landforms*, *41*(12), 1736–1757. https://doi.org/10.1002/esp.3947

Fox, M., Goren, L., May, D. A., & Willett, S. D. (2014). Inversion of fluvial channels for paleorock uplift rates in Taiwan. *Journal of Geophysical Research: Earth Surface*, *119*(9), 1853–1875. https://doi.org/10.1002/2014jf003196

Gallen, S. F., Wegmann, K. W., & Bohnenstiehl, D. W. R. (2013). Miocene rejuvenation of topographic relief in the southern Appalachians. *GSA Today*, *23*(2), 4–10. https://doi.org/10.1130/GSATG163A.1

Gasparini, N. M., & Whipple, K. X. (2014). Diagnosing climatic and tectonic controls on topography: Eastern flank of the northern Bolivian Andes. *Lithosphere*, *6*(4), 230–250. https://doi.org/10.1130/L322.1

Gasparini, N. M., Bras, R. L., & Whipple, K. X. (2006). Numerical modeling of non–steady-state river profile evolution using a sediment-flux-dependent incision model. In S. D. Willett, N. Hovius, M. T. Brandon, & D. M. Fisher (Eds.), *Tectonics, Climate, and Landscape Evolution* (Vol. 398, p. 0). Geological Society of America. https://doi.org/10.1130/2006.2398(08)

Gasparini, N. M., Whipple, K. X., & Bras, R. L. (2007). Predictions of steady state and transient landscape morphology using sediment-flux-dependent river incision models. *Journal of Geophysical*

Research: Earth Surface, *112*(3), 1–20. https://doi.org/10.1029/2006JF000567

Godard, V., Bourlès, D. L., Spinabella, F., Burbank, D. W., Bookhagen, B., Fisher, G. B., et al. (2014). Dominance of tectonics over climate in himalayan denudation. *Geology*, *42*(3), 243–246. https://doi.org/10.1130/G35342.1

Goren, L., Fox, M., & Willett, S. D. (2014). Tectonics from fluvial topography using formal linear inversion: Theory and applications to the Inyo Mountains, California. *Journal of Geophysical Research F: Earth Surface*, *119*(8), 1651–1681. https://doi.org/10.1002/2014JF003079

Granger, D. E., Kirchner, J. W., & Finkel, R. (1996). Spatially averaged long-term erosion rates measured from in situ-produced cosmogenic nuclides in alluvial sediment. *Journal of Geology*, *104*(3), 249–257. https://doi.org/10.1086/629823

Hack, J. T. (1957). *Studies of Longitudinal Stream Profiles in Virginia and Maryland*. Retrieved from https://pubs.usgs.gov/pp/0294b/report.pdf

Han, J., Gasparini, N. M., Johnson, J. P. L., & Murphy, B. P. (2014). Modeling the influence of rainfall gradients on discharge, bedrock erodibility, and river profile evolution, with application to the Big Island, Hawai'i. *Journal of Geophysical Research: Earth Surface*, *119*(6), 1418–1440. https://doi.org/10.1002/2013JF002961

Han, J., Gasparini, N. M., & Johnson, J. P. L. (2015). Measuring the imprint of orographic rainfall gradients on the morphology of steady-state numerical fluvial landscapes. *Earth Surface Processes and Landforms*, *40*(10), 1334–1350. https://doi.org/10.1002/esp.3723

Harel, M. A., Mudd, S. M., & Attal, M. (2016). Global analysis of the stream power law parameters based on worldwide 10Be denudation rates. *Geomorphology*, *268*, 184–196. https://doi.org/10.1016/j.geomorph.2016.05.035

Henck, A. C., Huntington, K. W., Stone, J. O., Montgomery, D. R., & Hallet, B. (2011). Spatial controls on erosion in the Three Rivers Region, southeastern Tibet and southwestern China. *Earth and Planetary Science Letters*, *303*(1–2), 71–83. https://doi.org/10.1016/j.epsl.2010.12.038

Howard, A. D. (1994). A detachment-limited model of drainage basin evolution. *Water Resources Research*, *30*(7), 2261–2285. https://doi.org/10.1029/94WR00757

Howard, A. D., & Kerby, G. (1983). Channel changes in badlands. *Geological Society of America Bulletin*, *94*, 739–752.

Insel, N., Ehlers, T. A., Schaller, M., Barnes, J. B., Tawackoli, S., & Poulsen, C. J. (2010). Spatial and temporal variability in denudation across the Bolivian Andes from multiple geochronometers.

Geomorphology, *122*(1–2), 65–77. https://doi.org/10.1016/j.geomorph.2010.05.014

Kirby, E., & Whipple, K. X. (2012). Expression of active tectonics in erosional landscapes. *Journal of Structural Geology*, *44*, 54–75. https://doi.org/10.1016/j.jsg.2012.07.009

Kober, F., Zeilinger, G., Hippe, K., Marc, O., Lendzioch, T., Grischott, R., et al. (2015). Tectonic and lithological controls on denudation rates in the central Bolivian Andes. *Tectonophysics*, *657*, 230–244. https://doi.org/10.1016/j.tecto.2015.06.037

Lague, D. (2014). The stream power river incision model: Evidence, theory and beyond. *Earth Surface Processes and Landforms*, *39*(1), 38–61. https://doi.org/10.1002/esp.3462

Miller, S. R., Sak, P. B., Kirby, E., & Bierman, P. R. (2013). Neogene rejuvenation of central Appalachian topography: Evidence for differential rock uplift from stream profiles and erosion rates. *Earth and Planetary Science Letters*, *369–370*(May), 1–12. https://doi.org/10.1016/j.epsl.2013.04.007

Molnar, P. (2001). Climate change, flooding in arid environments, and erosion rates. *Geology*, *29*(12), 1071–1074. https://doi.org/10.1130/0091-7613(2001)029<1071:CCFIAE>2.0.CO

Morell, K. D., Sandiford, M., Rajendran, C. P., Rajendran, K., Alimanovic, A., Fink, D., & Sanwal, J. (2015). Geomorphology reveals active décollement geometry in the central Himalayan seismic gap. *Lithosphere*, *7*(3), 247–256. https://doi.org/10.1130/L407.1

Murphy, B. P., Johnson, J. P. L., Gasparini, N. M., & Sklar, L. S. (2016). Chemical weathering as a mechanism for the climatic control of bedrock river incision. *Nature*, *532*(7598), 223–227. https://doi.org/10.1038/nature17449

Neely, A. B., & DiBiase, R. A. (2020). Drainage area, bedrock fracture spacing, and weathering controls on landscape-scale patterns in surface sediment grain size. *Earth and Space Science Open Archive*, 1–22. https://doi.org/10.1002/essoar.10502617.1

Olen, S. M., Bookhagen, B., & Strecker, M. R. (2016). Role of climate and vegetation density in modulating denudation rates in the Himalaya. *Earth and Planetary Science Letters*, *445*, 57–67. https://doi.org/10.1016/j.epsl.2016.03.047

Ouimet, W. B., Whipple, K. X., & Granger, D. E. (2009). Beyond threshold hillslopes: Channel adjustment to base-level fall in tectonically active mountain ranges. *Geology*, *37*(7), 579–582. https://doi.org/10.1130/G30013A.1

Perron, J. T. (2017). Climate and the Pace of Erosional Landscape Evolution. *Annual Review of Earth and Planetary Sciences*, *45*(1), 561–591. https://doi.org/10.1146/annurev-earth-060614-105405

974 Portenga, E. W., Bierman, P. R., Duncan, C., Corbett, L. B., Kehrwald, N. M., & Rood, D. H. (2015).
975 Erosion rates of the Bhutanese Himalaya determined using in situ-produced 10Be. *Geomorphology*,
976 *233*, 112–126. https://doi.org/10.1016/j.geomorph.2014.09.027

977 Reinhardt, L. J., Bishop, P., Hoey, T. B., Dempster, T. J., & Sanderson, D. C. W. (2007). Quantification
978 of the transient response to base-level fall in a small mountain catchment: Sierra Nevada, southern
979 Spain. *Journal of Geophysical Research: Earth Surface*, *112*(3).
980 https://doi.org/10.1029/2006JF000524

981 Riebe, C. S., Sklar, L. S., Lukens, C. E., & Shuster, D. L. (2015). Climate and topography control the size
982 and flux of sediment produced on steep mountain slopes. *Proceedings of the National Academy of*
983 *Sciences of the United States of America*, *112*(51), 15574–15579.
984 https://doi.org/10.1073/pnas.1503567112

985 Rigon, R., Rodriguez-Iturbe, I., Maritan, A., Giacometti, A., Tarboton, D. G., & Rinaldo, A. (1996). On
986 Hack's Law. *Water Resources Research*, *32*(11), 3367–3374. https://doi.org/10.1029/96WR02397

987 Riihimaki, C. A., Anderson, R. S., & Safran, E. B. (2007). Impact of rock uplift on rates of late Cenozoic
988 Rocky Mountain river incision. *Journal of Geophysical Research: Earth Surface*, *112*(3), 1–15.
989 https://doi.org/10.1029/2006JF000557

990 Rinaldo, A., Dietrich, W. E., Rigon, R., Vogel, G. K., & Rodrlguezlturbe, I. (1995). Geomorphological
991 signatures of varying climate. *Nature*, *374*(6523), 632–635. https://doi.org/10.1038/374632a0

992 Roe, G. H. (2005). Orographic Precipitation. *Annual Review of Earth and Planetary Sciences*, *33*(1), 645–
993 671. https://doi.org/10.1146/annurev.earth.33.092203.122541

994 Roe, G. H., Montgomery, D. R., & Hallet, B. (2002). Effects of orographic precipitation variations on the
995 concavity of steady-state river profiles. *Geology*, *30*(2), 143–146. https://doi.org/10.1130/0091-
996 7613(2002)030<0143:EOOPVO>2.0.CO;2

997 Roe, G. H., Montgomery, D. R., & Hallet, B. (2003). Orographic precipitation and the relief of mountain
998 ranges. *Journal of Geophysical Research: Solid Earth*, *108*(B6).
999 https://doi.org/10.1029/2001jb001521

1000 Roe, G. H., Whipple, K. X., & Fletcher, J. K. (2008). Feedbacks among climate, erosion, and tectonics in
1001 a critical wedge orogen. *American Journal of Science*, *308*(7), 815–842.
1002 https://doi.org/10.2475/07.2008.01

1003 Royden, L., & Perron, J. T. (2013). Solutions of the stream power equation and application to the
1004 evolution of river longitudinal profiles. *Journal of Geophysical Research: Earth Surface*, *118*(2),

497–518. https://doi.org/10.1002/jgrf.20031

Safran, E. B., Bierman, P. R., Aalto, R., Dunne, T., Whipple, K. X., & Caffee, M. (2005). Erosion rates driven by channel network incision in the Bolivian Andes. *Earth Surface Processes and Landforms*, *30*(8), 1007–1024. https://doi.org/10.1002/esp.1259

Scherler, D., Bookhagen, B., & Strecker, M. R. (2014). Tectonic control on 10Be-derived erosion rates in the Garhwal Himalaya, India. *Journal of Geophysical Research: Earth Surface*, *119*(2), 83–105. https://doi.org/10.1002/2013JF002955

Scherler, D., DiBiase, R. A., Fisher, G. B., & Avouac, J. P. (2017). Testing monsoonal controls on bedrock river incision in the Himalaya and Eastern Tibet with a stochastic-threshold stream power model. *Journal of Geophysical Research: Earth Surface*, *122*(7), 1389–1429. https://doi.org/10.1002/2016JF004011

Schoenbohm, L. M., Whipple, K. X., Burchfiel, B. C., & Chen, L. (2004). Geomorphic constraints on surface uplift, exhumation, and plateau growth in the Red River region, Yunnan Province, China. *Bulletin of the Geological Society of America*, *116*(7–8), 895–909. https://doi.org/10.1130/B25364.1

Sklar, L. S., Riebe, C. S., Marshall, J. A., Genetti, J., Leclere, S., Lukens, C. L., & Merces, V. (2017). The problem of predicting the size distribution of sediment supplied by hillslopes to rivers. *Geomorphology*, *277*, 31–49. https://doi.org/10.1016/j.geomorph.2016.05.005

Tucker, G E, & Whipple, K. X. (2002). Topographic outcomes predicted by stream erosion models: Sensitivity analysis and intermodel comparison. *Journal of Geophysical Research: Solid Earth*, *107*(B9), ETG 1-1-ETG 1-16. https://doi.org/10.1029/2001jb000162

Tucker, Gregory E., & Slingerland, R. (1997). Drainage basin responses to climate change. *Water Resources Research*, *33*(8), 2031–2047. https://doi.org/10.1029/97WR00409

Vanacker, V., von Blanckenburg, F., Govers, G., Molina, A., Campforts, B., & Kubik, P. W. (2015). Transient river response, captured by channel steepness and its concavity. *Geomorphology*, *228*, 234–243. https://doi.org/10.1016/j.geomorph.2014.09.013

Ward, D. J., & Galewsky, J. (2014). Exploring landscape sensitivity to the Pacific Trade Wind Inversion on the subsiding island of Hawaii. *Journal of Geophysical Research: Earth Surface*, *119*(9), 2048–2069. https://doi.org/10.1002/2014JF003155

Whipple, K. X. (2001). Fluvial landscape response time: How plausible is steady-state denudation? *American Journal of Science*, *301*(4–5), 313–325. https://doi.org/10.2475/ajs.301.4-5.313

Whipple, K. X., & Meade, B. J. (2006). Orogen response to changes in climatic and tectonic forcing.

Earth and Planetary Science Letters, *243*(1–2), 218–228. https://doi.org/10.1016/j.epsl.2005.12.022

Whipple, K. X., & Tucker, G. E. (1999). Dynamics of the stream-power river incision model: Implications for height limits of mountain ranges, landscape response timescales, and research needs. *Journal of Geophysical Research: Solid Earth*, *104*(B8), 17661–17674. https://doi.org/10.1029/1999jb900120

Whipple, K. X., & Tucker, G. E. (2002). Implications of sediment-flux-dependent river incision models for landscape evolution. *Journal of Geophysical Research*, *107*(B2), 2039. https://doi.org/10.1029/2000jb000044

Whittaker, A. C. (2012). How do landscapes record tectonics and climate? *Lithosphere*, *4*(2), 160–164. https://doi.org/10.1130/RF.L003.1

Whittaker, A. C., Cowie, P. A., Attal, M., Tucker, G. E., & Roberts, G. P. (2007). Bedrock channel adjustment to tectonic forcing: Implications for predicting river incision rates. *Geology*, *35*(2), 103–106. https://doi.org/10.1130/G23106A.1

Willenbring, J. K., Gasparini, N. M., Crosby, B. T., & Brocard, G. (2013). What does a mean mean? The temporal evolution of detrital cosmogenic denudation rates in a transient landscape. *Geology*, *41*(12), 1215–1218. https://doi.org/10.1130/G34746.1

Wittmann, H., Malusà, M. G., Resentini, A., Garzanti, E., & Niedermann, S. (2016). The cosmogenic record of mountain erosion transmitted across a foreland basin: Source-to-sink analysis of in situ 10Be, 26Al and 21Ne in sediment of the Po river catchment. *Earth and Planetary Science Letters*, *452*, 258–271. https://doi.org/10.1016/j.epsl.2016.07.017

Wobus, C., Whipple, K. X., Kirby, E., Snyder, N., Johnson, J., Spyropolou, K., et al. (2006). Tectonics from topography: Procedures, promise, and pitfalls. *Special Paper of the Geological Society of America*, *398*(04), 55–74. https://doi.org/10.1130/2006.2398(04)

Figures and Tables

Table 1. Model Parameters

Parameters	Value	Units
U	5.0×10^{-4}	$m \cdot yr^{-1}$
K_p	2.5×10^{-9}	$m^{-1} \cdot yr^{-1}$
m	1	
n	2	

k_a	6.69	
h	1.67	
L		
Trunk	50	km
Tributaries	5	km
A		
Trunk	472	km^2
Tributaries	11	km^2
A_c	1	km^2
Node spacing	25	m
Time step	50	yr
Tributary Spacing	1	km

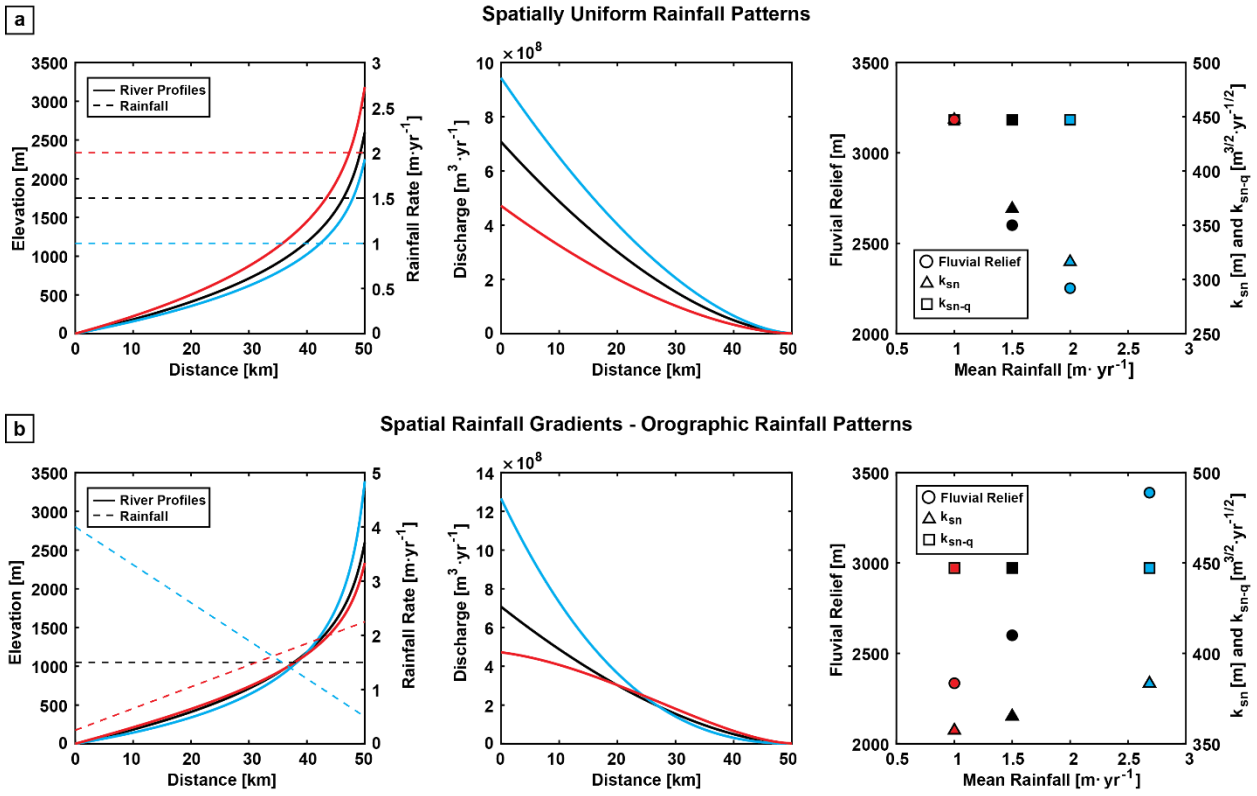

Figure 1. Influence of rainfall on channel profile form and topographic metrics at steady state. a) Top row – left panel shows river profiles adjusted to spatially uniform 1, 1.5, and 2 m/yr of rainfall (dashed, solid, and dotted, respectively). Corresponding discharge accumulation curves are shown in the middle panel. Right panel shows the relationship between mean rainfall (defined as Q/A) calculated at the outlet, with fluvial relief (R), k_{sn}, and $k_{sn\text{-}q}$ for a fixed uniform rock uplift rate. Note, at steady state fluvial relief and k_{sn} are inversely related to mean rainfall, while $k_{sn\text{-}q}$ is independent of changes in rainfall. b) Bottom row – all panels as in (a) but for a comparable suite of steady-state profiles adjusted to uniform 1.5 m/yr of rainfall, rainfall decreasing upstream from 4 to 0.5 m/yr, and rainfall increasing upstream from 0.25 to 2.25 m/yr.

Note intersections that occur between profiles in the left panel, and in downstream discharge (middle panel), and that fluvial relief and k_{sn} are positively related to mean rainfall in these cases (right panel), inverted from (a). All other model parameters are equal (see Table 1).

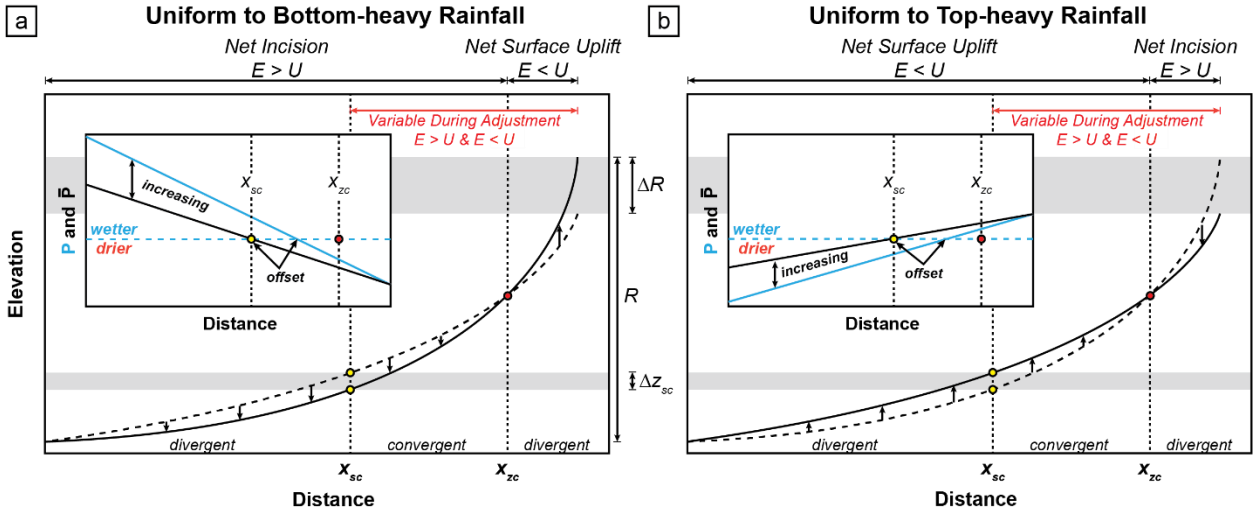

Figure 2. Schematic illustration of key aspects of complex transient river profile responses – defined in section 3.3 – that can result due to changes from spatially uniform rainfall (initial) to a bottom-heavy (a) and top-heavy rainfall gradient (b) – rainfall shown in inset. Initial and final steady state river profiles shown in dashed and solid black lines, respectively. Horizontal grey bars highlight net change in fluvial relief (ΔR) and the maximum amount of enhanced incision (Δz_{sc}) along the profile due to change in rainfall. Colored circles mark positions of x_{sc} (yellow) and x_{zc} (red) – see text for definition and discussion of these points – that also demarcate segments of net divergent and convergent transient adjustments. Domains of net mode of transient adjustment indicated along top axis. Note reversal at position x_{zc} (net incision downstream, net uplift upstream); however, during transience, adjustment upstream of x_{sc} is variable with time. Inset shows both initial local rainfall rate (P) and upstream averaged rainfall ($\overline{P}$) in blue dashed line; $P = \overline{P}$ for spatially uniform rainfall. Solid lines show final local rainfall rate (blue) and final upstream averaged rainfall (black). Positions of x_{sc} and x_{zc} in inset correspond to those along the profiles in the main figure. Note along-stream offset in position where P and $\overline{P}$ exceed the initial rainfall rate, the latter corresponding to x_{sc}. Also, note that the difference between P and $\overline{P}$ increases systematically downstream.

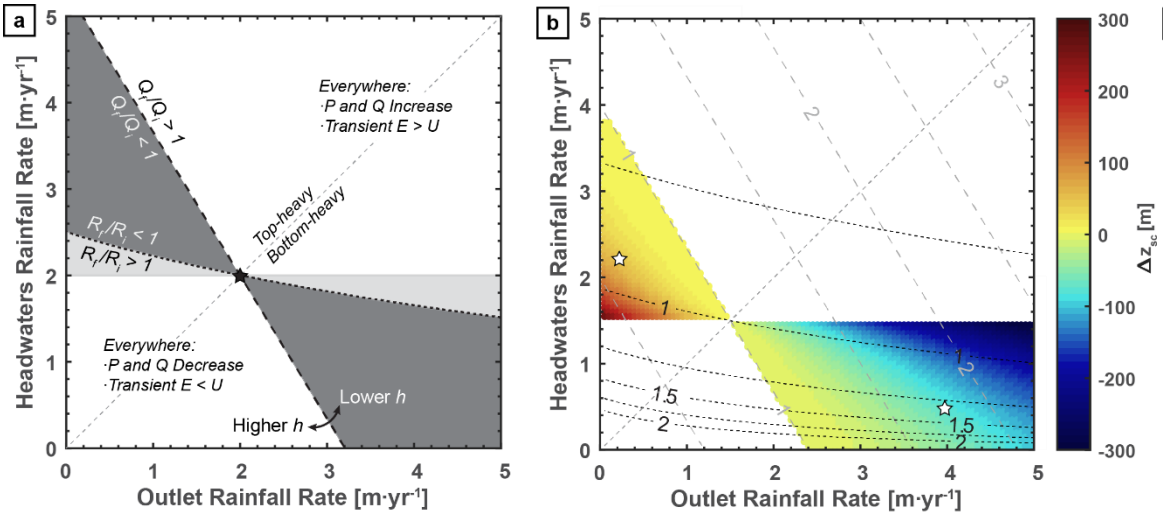

Figure 3. Sensitivity analysis of a river profile to different spatial gradients in rainfall. a) Defines general domains of behavior described in the sensitivity analysis shown in (b) – see text for descriptions of different fields. Black star in (a) marks the initial condition; note, initial conditions in panels (a) and (b) are different. Top-heavy and bottom-heavy domains are separated by the 1:1 line. The primary influence of different h values in Hack's relationship is on the slope of Q_f/Q_i, as indicated. b) Same as (a) but where the initial profile is adjusted to spatially uniform P = 1.5 m/yr, as in Figure 1, and grey fields in (a) are colored by magnitude of Δz_{sc} (e.g., Figure 2; see text for more discussion). White stars show rainfall gradient scenarios explored in section 3 – Cases 3 & 4. Contours of Q_f/Q_i are shown in grey dashed lines, and contours of R_f/R_i in black dotted lines.

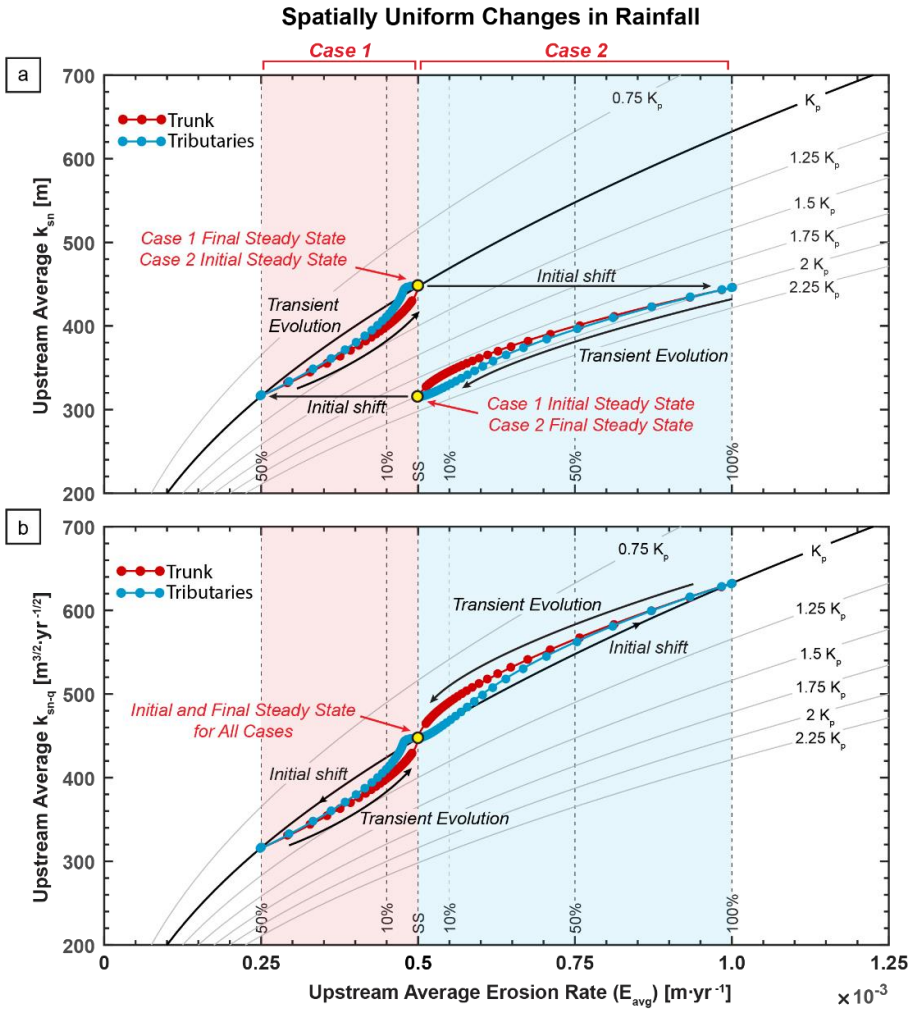

Figure 4. Representative time slice of transient evolution for Case 1 (uniform decrease in rainfall from 2 m/yr to 1 m/yr) and Case 2 (uniform increase in rainfall from 1 m/yr to 2 m/yr) through (a) k_{sn}-E_{avg} and (b) $k_{sn\text{-}q}$-E_{avg} parameter spaces. Case 1 is shown in red shaded domain (transient decrease in erosion rate, $E < U$), and Case 2 is in blue shaded domain (transient increase in erosion rate, $E > U$). Curves expressing the expected steady state relationship between channel steepness and erosion rate with different uniform erosional efficiencies are shown; $K = K_p$, shown in black solid line, and grey lines show different values of K as multiples of K_p. Vertical dashed lines show percent deviations from steady state erosion rate. Initial and final conditions shown with yellow circles, as labelled. Model data from different positions along the trunk profile and individual tributaries shown with red and blue data points, respectively. Trunk data shown are only profile nodes at tributary junctions – all trunk profile datapoints have a corresponding tributary datapoint at the same position within the modelled landscape. Trunk profile data show upstream mean values from their respective position, and tributary data show mean values for the entire tributary profile (i.e., at the junction with the trunk profile).

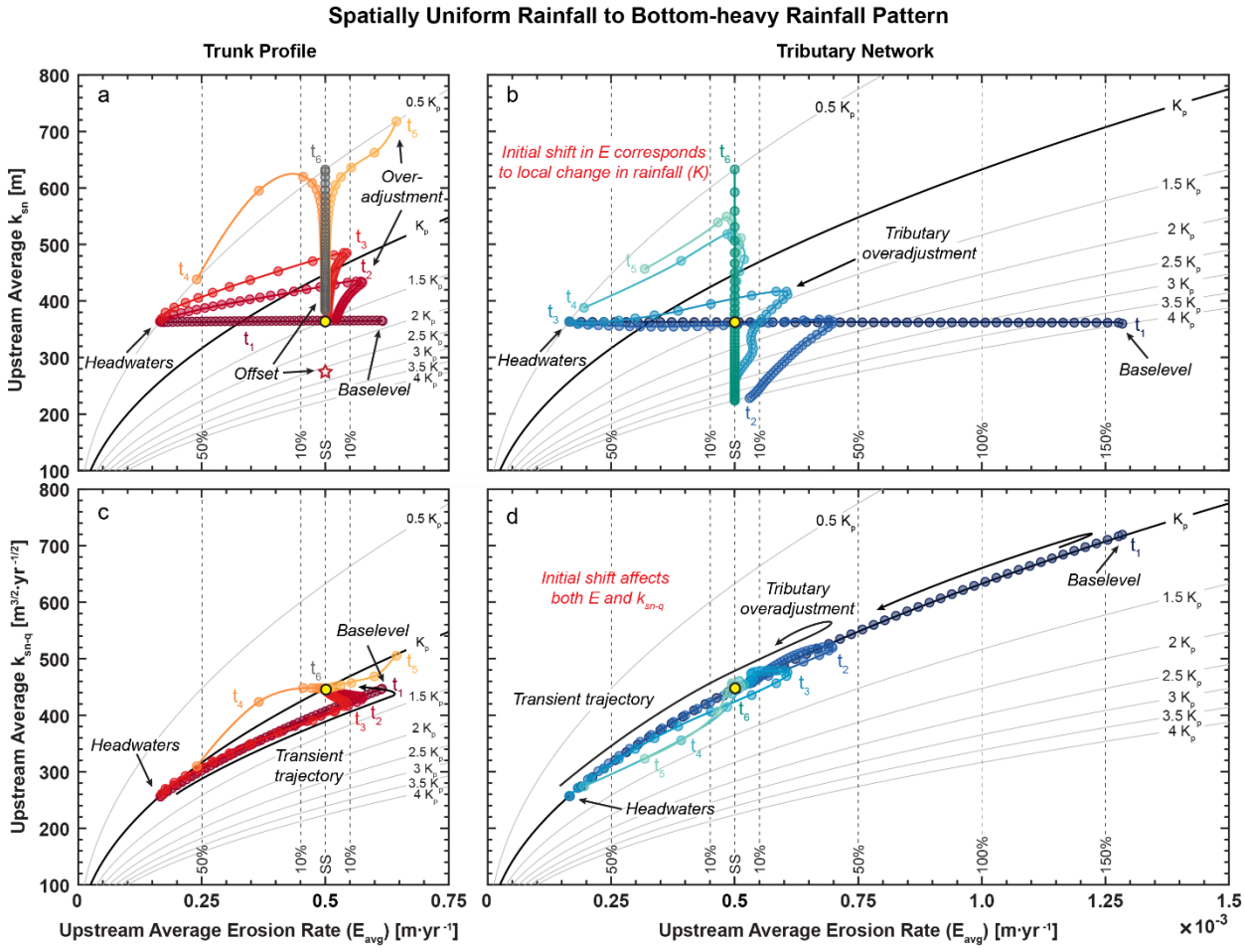

Figure 5. Transient evolution of the trunk profile (a & c) and network of tributaries (b & d) in Case 3 (spatially uniform P = 1.5 m/yr to gradient decreasing upstream from 4 to 0.5 m/yr) through k_{sn}-E_{avg} (a & b) and k_{sn-q}-E_{avg} (b & d) parameter spaces. Layout of individual panels is like Figure 4. Six representative time slices are shown; t_1 shows time at 10 kyr model time (i.e., first time step at following change in rainfall), t_6 is at final steady state. Time intervals are not evenly spaced, but t_1-t_6 are the same time-step for all panels. Note range in k_{sn} values, and related erosional efficiency values, spanned at final steady state in panels (a) and (b). Also, the range of responses by trunk profile during transient adjustment is significantly reduced relative to the network of tributaries in both k_{sn} and k_{sn-q}. Star in panel (a) shows expected erosional efficiency calculated from equation (1b) based on the final mean rainfall of 2.68 m/yr (2.68·K_p) at steady state, which corresponds to a predicted mean k_{sn} of ~275. Note offset between this value and range of erosional efficiency and k_{sn} values spanned by trunk profile.

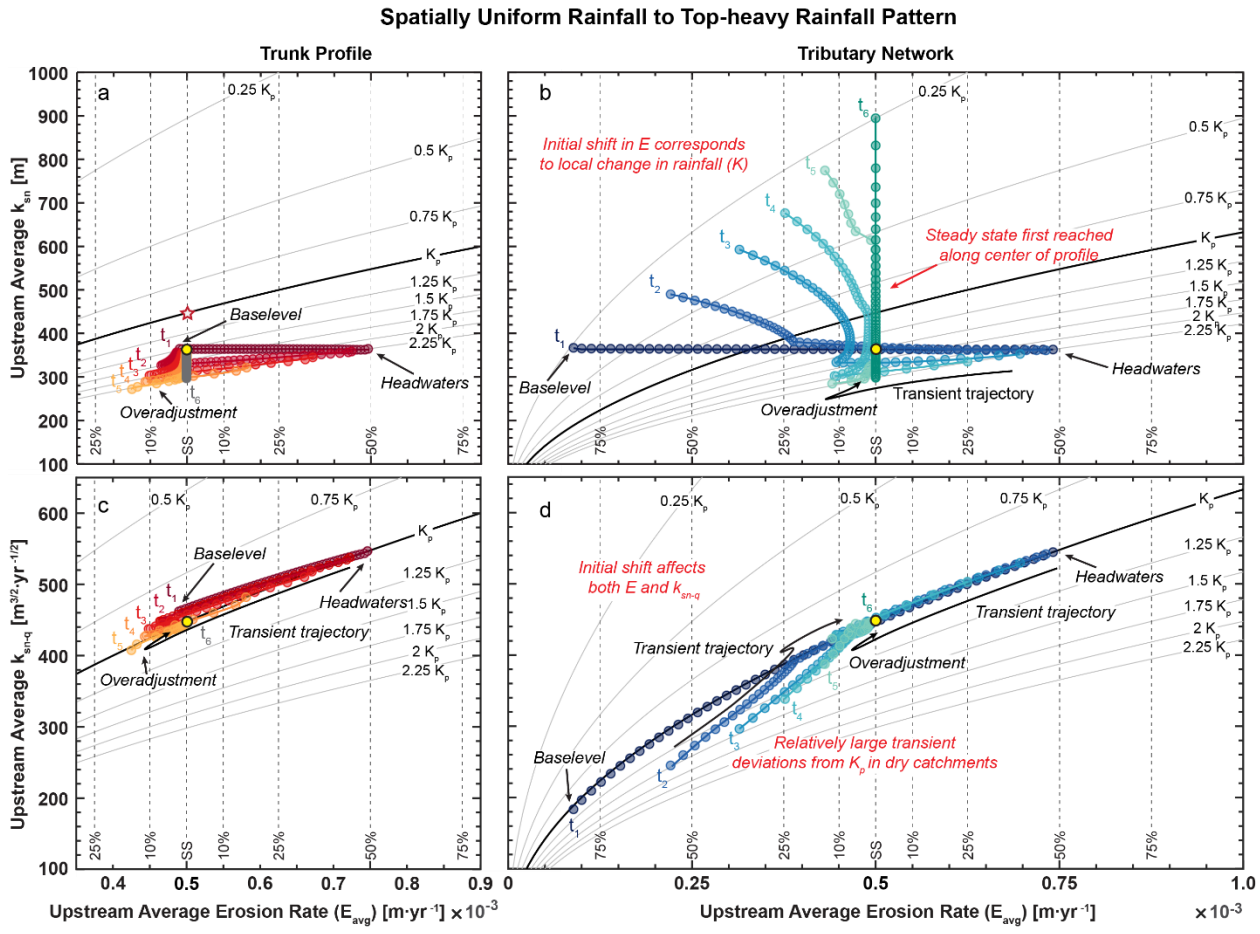

Figure 6. Transient evolution of the trunk profile (a & c) and network of tributaries (b & d) in Case 4 (spatially uniform P = 1.5 m/yr to gradient increasing upstream from 0.25 to 2.25 m/yr) through k_{sn}-E_{avg} (a & b) and k_{sn-q}-E_{avg} (c & d) parameter spaces; figure layout is same as Figure 5. Like Case 3, the range in k_{sn} and k_{sn-q} values in trunk stream response is significantly less than in the network of tributaries. However, note relatively larger disparity between the range k_{sn} and erosional efficiency (K) spanned by the trunk profile and the network of tributaries at final steady state (a & b). Transient deviations from curve for K_p in panel (d) are also relatively larger than in Case 3, which is consistent with the fact that these tributaries are much drier – discussed further in section 5.1. Star in panel (a) shows K calculated from equation (1b) based on the final mean rainfall of 1 m/yr ($K = K_p$) at steady state, which corresponds to a predicted mean k_{sn} of ~450. Again, note offset between this value and range of erosional efficiency and k_{sn} values spanned by trunk profile.

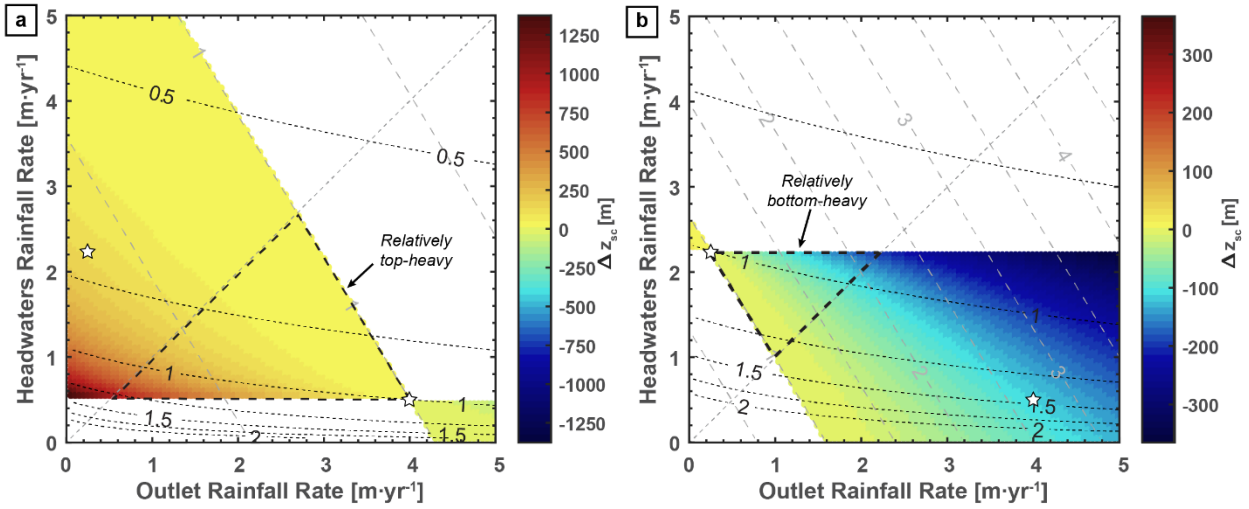

Figure 7. Sensitivity analysis where initial conditions are rainfall patterns used in Case 3 (a) bottom heavy – decreasing upstream from 4 to 0.5 m/yr – and top heavy gradient from Case 4 (b) – increasing upstream from 0.25 to 2.25 m/yr. Panel layouts are the same as in Figure 3b. Triangular fields demarcated in black dashes bound rainfall gradients with the same pattern as the initial condition (i.e., bottom-heavy or top-heavy), but cause complex transient responses similar to those expected for reversals in polarity of the rainfall pattern as the rainfall becomes *relatively* more or less bottom- or top-heavy – see section 5.1 for further discussion.

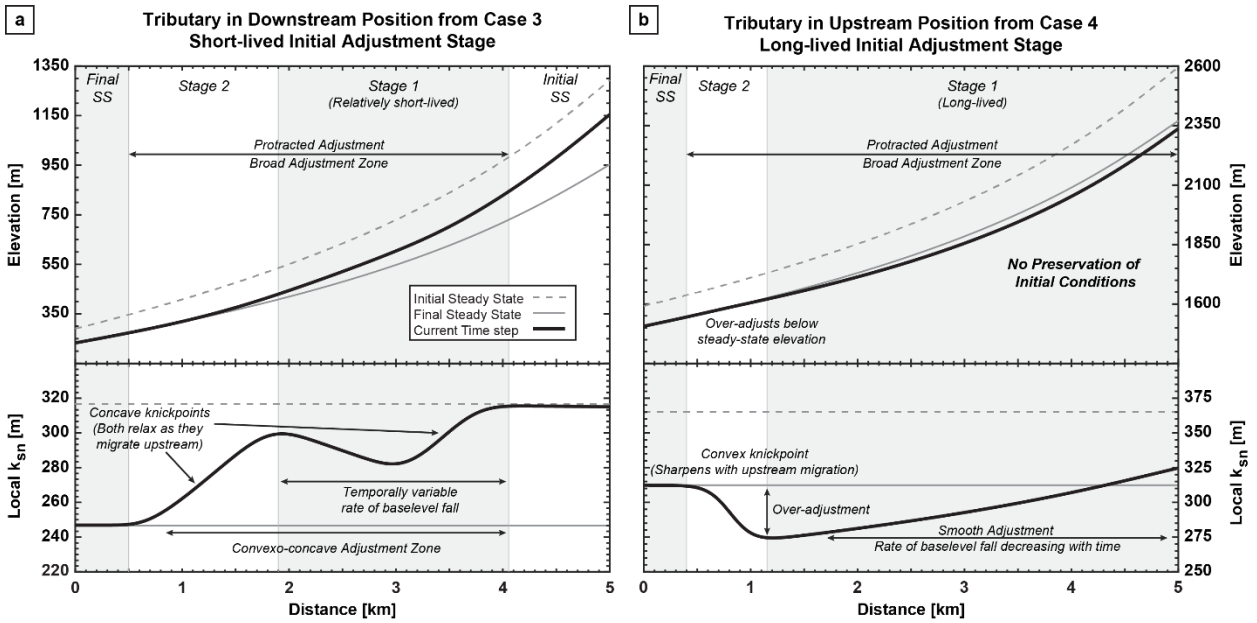

Figure 8. Representative examples of multi-stage tributary response in Cases 3 (a) & 4 (b). Note, upstream positions always experience relatively longer initial adjustment stages than downstream positions, regardless of rainfall gradient. Grey shaded and white regions show where initial and final steady states (SS) and different adjustment stages are represented along the profile lengths, as indicated across top axis. a) Shows a tributary located in a relatively downstream position, 15 km from trunk outlet ($x < x_{sc}$) and 300 kyr into transient adjustment of the catchment in Case 3, where the initial adjustment stage is relatively short-lived. Despite this, protracted adjustment creates a several-kilometer-wide adjustment zone with relatively smooth but notable along-stream variations in k_{sn}. This pattern is subtle on the longitudinal profile. b) Shows a tributary located in an upstream position, 45 km from the trunk outlet ($x > x_{sc}$) and 1.725 Myr into transient adjustment of the catchment in Case 4, where the initial adjustment stage is long-lived. The initial adjustment stage reshapes the entire profile prior to adjustment of the trunk profile, but no transient knickpoints or other obvious topographic indicators of such significant modification are present, with smoothly varying local k_{sn} values within 10% of the mean. Also, note overadjustment means that the increase in channel steepness required to reach steady state contrasts with net reduction in channel steepness during transient adjustment.

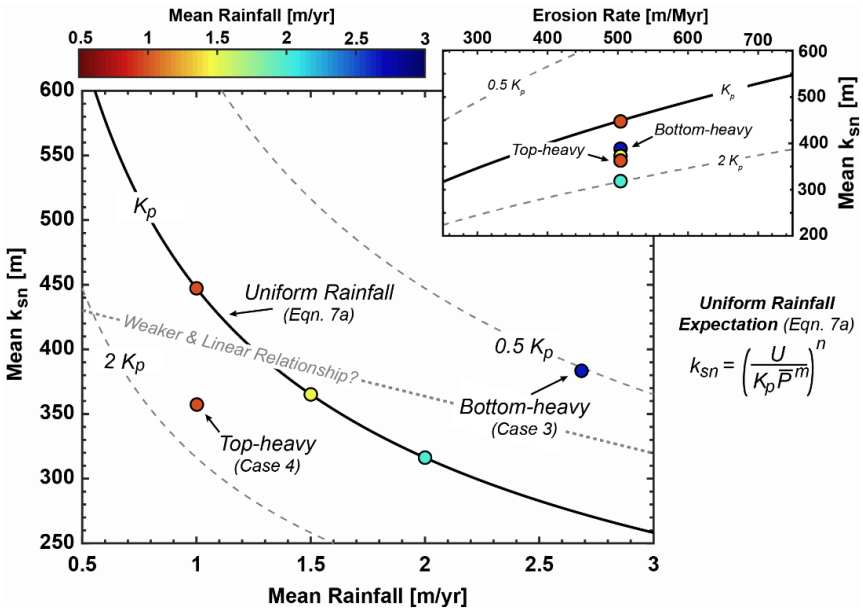

Figure 9. Plot illustrating how rainfall gradients systematically influence correlation between mean rainfall and k_{sn} at steady state, and consequences for relationship between channel steepness and erosion rate (inset). A common symbology is used in both the main figure and the inset. Expected SPM relationship based on uniform climate (uniform erosional efficiency, K) from equation 7a is shown in solid back line. Grey long-dashed lines represent changes in $K = K_p P^m$ by factors of two, which correspond to uniform changes in mean rainfall and erosional efficiency of the same magnitude (m = 1). Circles colored by mean rainfall reflect scenarios shown in Figure 1 – uniform rainfall of 1, 1.5, and 2 m/yr, and top- and bottom-heavy gradients (labeled as Case 4 and Case 3). While K_p is uniform in all scenarios, rainfall gradients cause dispersion (apparent differences in erosional efficiency) from the expected relationship (solid black line) equivalent to differences in K_p of approximately a factor of two (inset). For instance, the bottom-heavy case where mean rainfall is ~2.7 m/yr exhibits an apparent ~50% reduction in erosional efficiency based on mean k_{sn} (plots on $K \approx 0.5K_p$ curve in main figure) and thus plots where one would expect a catchment that experiences half as much rainfall to plot in the inset. Dotted line in main figure illustrates, conceptually, how this dispersion could distort inferred relationships between mean rainfall and channel steepness (weaker and quasi-linear in this case), even at steady state and in systems where the SPM is a complete description of the controls on channel profile form. Where uplift rates are unknown, this systematic bias in apparent erosional efficiency due to rainfall gradients is a potential source of dispersion in relationships between k_{sn} and erosion rate (inset), which in and of itself can obscure or distort the importance of variations in rainfall on channel steepness and erosion rates.

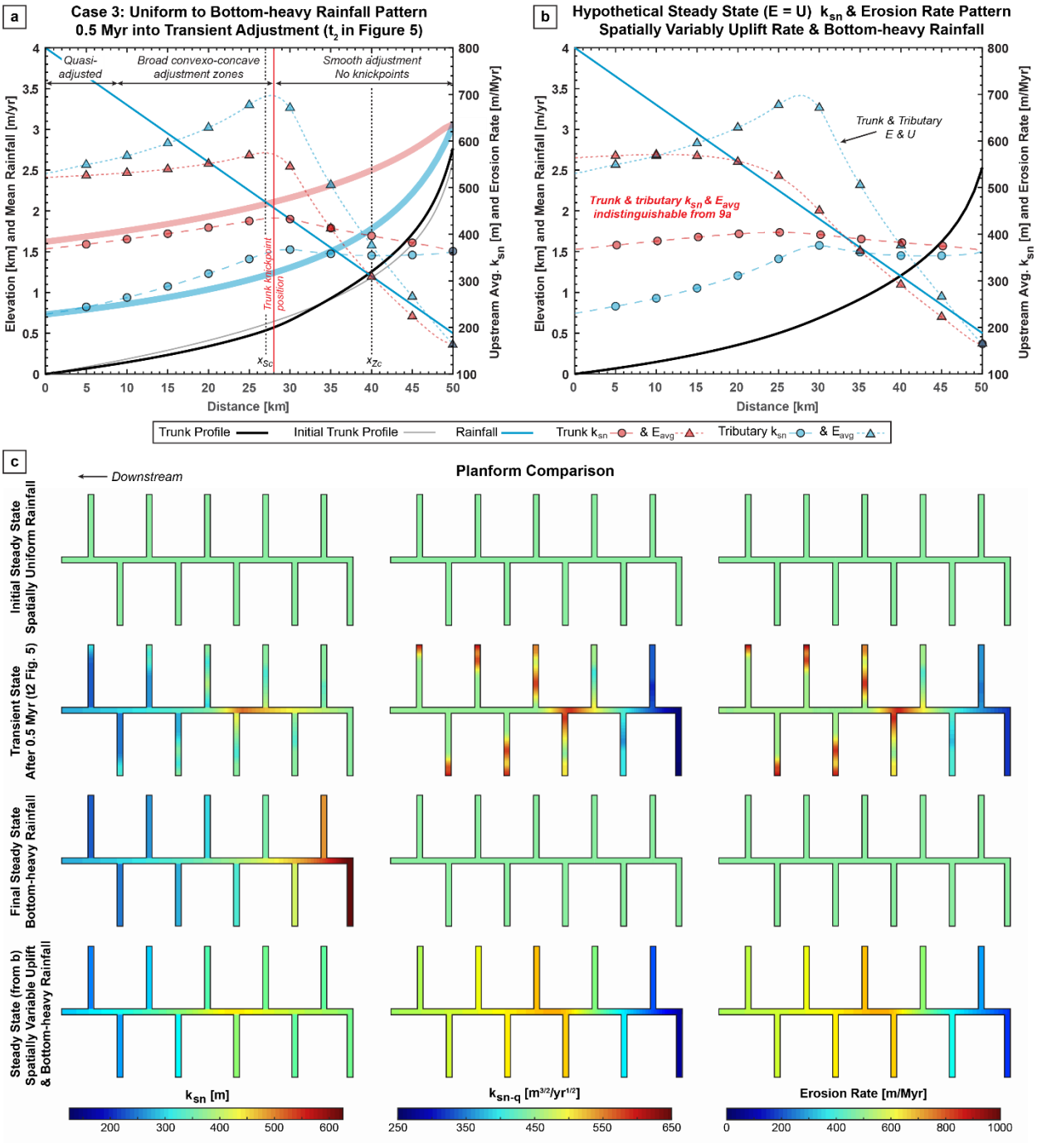

Figure 10. Illustration of potentially misleading spatial patterns that arise among channel steepness, rainfall, and erosion rates during transient adjustment to a change in rainfall pattern, particularly when erosion rate and morphometrics are averaged at catchment scale as is common – see section 5.1.2 for detailed discussion. a) Shows time slice at 0.5 Myr into transient adjustment of Case 3 (t_2 in Figure 5). For clarity, a subsample of ten data points is shown for each model dataset; connecting dashed line is populated from full model. Thick colored bands (red for trunk stream, blue for tributaries) show final steady state upstream-averaged k_{sn} pattern toward which the modelled landscape is adjusting. Position of

trunk knickpoint, defined as upstream extent of quasi-steady state adjustment, is shown by red solid line (compares with panel c). Zones describing morphological characteristics of tributary catchments are shown across the top axis (compare with panel c). b) Modelled steady state k_{sn} and erosion rate pattern of a catchment experiencing a bottom-heavy rainfall gradient and a spatial gradient in uplift rate that matches the catchment-averaged tributary erosion rates in panel a). c) Shows planform development of local k_{sn}, $k_{sn\text{-}q}$, and erosion rates at initial and final steady states, a transient time slice from Case 3, and steady state pattern from (b). Downstream is to the left, as indicated. Transient time slice and tributaries are the same as in panels (a & b). Note that trunk and tributary profiles are not illustrated to scale (Table 1). Importantly, we note here that while catchment-mean data (and arguably along-stream k_{sn}) can be indistinguishable between the transient and spatial uplift gradient scenarios, the expected patterns of erosion rate and $k_{sn\text{-}q}$ are distinct.